Immunity

# Plasmacytoid dendritic cell activation is dependent on coordinated expression of distinct amino acid transporters

## Graphical abstract

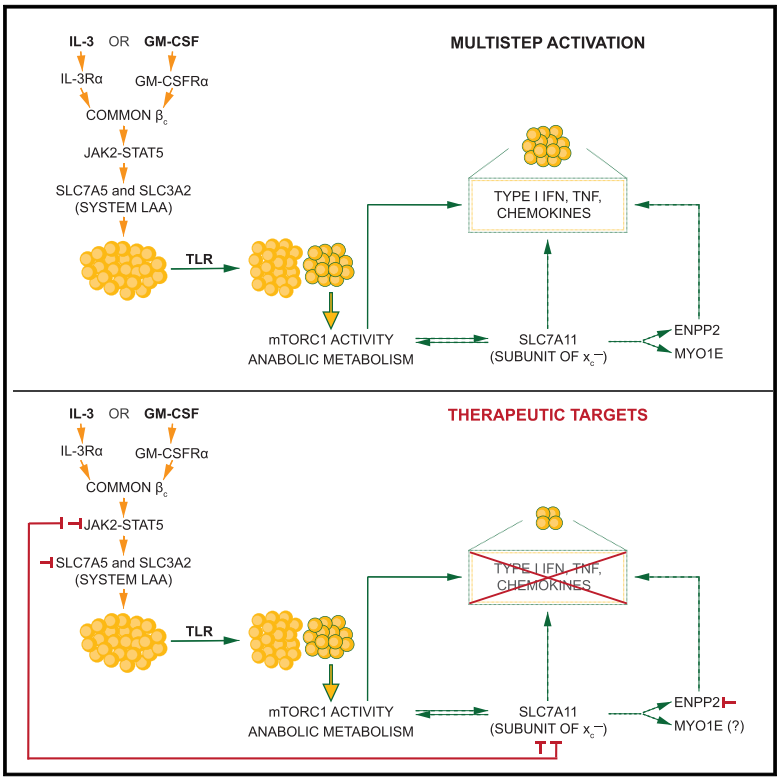


## Highlights

- IL-3 induces JAK2-STAT5-dependent expression of *SLC7A5* and *SLC3A2* in pDCs
- Leucine uptake via SLC7A5 and SLC3A2 primes mTORC1 for activation by TLR agonists
- pDCs activated by TLR agonists express *SLC7A11* and *ENPP2*
- Inhibitors of JAK2, SLC7A5, SLC7A11, and ENPP2 prevent cytokine production by pDCs

## Authors

Katarzyna M. Grzes, David E. Sanin, Agnieszka M. Kabat, ..., Mario Fabri, Erika L. Pearce, Edward J. Pearce

## Correspondence

epearce7@jhmi.edu

## In brief

The mechanism by which IL-3 supports human pDC biology is unclear. Grzes et al. show that IL-3 induces system L amino acid transporter expression, thereby priming mTORC1 to allow metabolic upregulation and cytokine production in response to TLR agonists.

Grzes et al., 2021, Immunity *54*, 2514–2530
November 9, 2021 
https://doi.org/10.1016/j.immuni.2021.10.009

CellPress

CellPress

Immunity

Article

# Plasmacytoid dendritic cell activation is dependent on coordinated expression of distinct amino acid transporters

Katarzyna M. Grzes,[1,7] David E. Sanin,[1,7] Agnieszka M. Kabat,[1] Michal A. Stanczak,[1,7] Joy Edwards-Hicks,[1] Mai Matsushita,[1] Alexandra Hackl,[1] Fabian Hässler,[1] Kristin Knoke,[2] Sophie Zahalka,[3,4] Matteo Villa,[1] David M. Kofler,[5] Reinhard E. Voll,[6] Paola Zigrino,[2] Mario Fabri,[2] Erika L. Pearce,[1,7,8] and Edward J. Pearce[1,7,9,10,11,*]

[1]Max Planck Institute for Immunobiology and Epigenetics, Freiburg 79108, Germany
[2]Department of Dermatology, University of Cologne, Cologne 50931, Germany
[3]Research Laboratory of Infection Biology, Department of Medicine I, Medical University of Vienna, Vienna 1090, Austria
[4]CeMM, Research Center for Molecular Medicine of the Austrian Academy of Sciences, Vienna 1090, Austria
[5]Department I of Internal Medicine, University of Cologne, Cologne 50931, Germany
[6]Department of Rheumatology and Clinical Immunology, Medical Center – University of Freiburg, Faculty of Medicine, University of Freiburg, Freiburg 79106, Germany
[7]Bloomberg-Kimmel Institute for Cancer Immunotherapy, Department of Oncology, Johns Hopkins University School of Medicine, Baltimore, MD 21287, USA
[8]Department of Biochemistry and Molecular Biology, Johns Hopkins University Bloomberg School of Public Health, Baltimore, MD 21287, USA
[9]Faculty of Biology, University of Freiburg, Freiburg 79104, Germany
[10]Department of Molecular Microbiology and Immunology, Johns Hopkins University Bloomberg School of Public Health, Baltimore, MD 21287, USA
[11]Lead contact
*Correspondence: epearce7@jhmi.edu
https://doi.org/10.1016/j.immuni.2021.10.009

## SUMMARY

Human plasmacytoid dendritic cells (pDCs) are interleukin-3 (IL-3)-dependent cells implicated in autoimmunity, but the role of IL-3 in pDC biology is poorly understood. We found that IL-3-induced Janus kinase 2-dependent expression of SLC7A5 and SLC3A2, which comprise the large neutral amino acid transporter, was required for mammalian target of rapamycin complex 1 (mTORC1) nutrient sensor activation in response to toll-like receptor agonists. mTORC1 facilitated increased anabolic activity resulting in type I interferon, tumor necrosis factor, and chemokine production and the expression of the cystine transporter SLC7A11. Loss of function of these amino acid transporters synergistically blocked cytokine production by pDCs. Comparison of *in vitro*-activated pDCs with those from lupus nephritis lesions identified not only SLC7A5, SLC3A2, and SLC7A11 but also ectonucleotide pyrophosphatase-phosphodiesterase 2 (ENPP2) as components of a shared transcriptional signature, and ENPP2 inhibition also blocked cytokine production. Our data identify additional therapeutic targets for autoimmune diseases in which pDCs are implicated.

## INTRODUCTION

Plasmacytoid dendritic cells (pDCs) reside in blood and lymphoid organs (Jegalian et al., 2009) but during inflammation they enter tissues where they serve as a major source of type I interferons (IFNs) (Cella et al., 1999; Liu, 2005; Siegal et al., 1999). They play a role during viral infections (Colonna et al., 2004; Reizis, 2019) and are implicated in autoimmune diseases like systemic lupus erythematosus (SLE) (Baccala et al., 2013; Blanco et al., 2001; Cederblad et al., 1998; Sisirak et al., 2014). SLE is a life-threatening disease that can affect multiple organs (Maidhof and Hilas, 2012). Its etiology is complex, but the over-production of IFN-α by activated pDCs is thought to be central to the development of disease. The development of therapeutic approaches that target IFN-α and its receptor are part of an ongoing effort to improve SLE treatment (Morand et al., 2020; Murphy and Isenberg, 2019). The primary mechanism of activation of pDCs is through ligation of endosomal Toll-like receptor (TLR) 7 or TLR9 by their nucleic acid agonists (Gilliet et al., 2008). Physiologically, access of nucleic acid ligands to these TLRs is promoted by the uptake of nucleic-acid-containing immune complexes (Lande et al., 2007). Downstream of TLRs, type-I IFNs are induced through an MyD88-IFN regulatory factor 7-dependent pathway, but further signaling through MYD88-dependent NFκ-B activation leads to the additional production of tumor necrosis factor (TNF) (Karrich et al., 2014). In addition, activated pDCs produce

chemokines (Piqueras et al., 2006), which can contribute to the development of SLE (Liao et al., 2016).

From their initial discovery, pDCs have been recognized to express high amounts of interleukin-3 receptor α (IL-3Rα, encoded by *IL3RA*) compared to other leukocytes (Olweus et al., 1997). Cultures of human pDCs incorporate IL-3 as a growth and survival factor (Ghirelli et al., 2010; Grouard et al., 1997), although this is not the case for mouse pDCs, which do not express the IL-3Rα (Swiecki and Colonna, 2015). IL-3 along with granulocyte-macrophage colony-stimulating factor (GM-CSF) and IL-5 are members of the common β chain ($\beta_c$) cytokine family (Dougan et al., 2019). Binding of cytokines to their respective cytokine-specific α subunits results in dimerization with common $\beta_c$, which initiates signaling through Janus kinase 2 (JAK2), which phosphorylates signal transducer and activator of transcription 5 (STAT5), causing translocation of STAT5 to the nucleus and initiation of transcription. A correlation between elevated IL-3 and SLE incidents has been noted (Fishman et al., 1993; Gottschalk et al., 2015), and there is a link between an IL-3-stimulated gene signature and the type-I IFN-stimulated gene signature in SLE patients (Oon et al., 2019). Monoclonal antibodies directed against IL-3Rα have been shown to diminish responses by human pDCs to TLR7 or TLR9 stimulation and to selectively deplete these cells from peripheral blood mononuclear cells (PBMCs) (Oon et al., 2016). Despite the strong association of IL-3 with pDC activation and SLE, the nature of the effect of IL-3 on pDCs is unclear.

IL-3 is the prototypic example of a cytokine acting as a growth factor to promote anabolic metabolism to support cellular growth and proliferation (Bauer et al., 2004; Vander Heiden et al., 2001). Previous work indicates that the production of IFN-α by pDCs is linked to changes in cell-intrinsic metabolism (Bajwa et al., 2016; Basit et al., 2018; Cao et al., 2008; Wu et al., 2016). In this context, the mammalian target of rapamycin complex 1 (mTORC1)-inhibitor rapamycin has been found to reduce IFN-α production by TLR9-activated human pDCs (Cao et al., 2008). mTORC1 is a serine/threonine protein kinase that regulates anabolic processes such as glycolysis, lipid synthesis, and protein translation (Saxton and Sabatini, 2017). The kinase activity of mTORC1 depends on the availability of nutrients like amino acids or glucose, and in this way, mTORC1 effectively couples upstream fuel sufficiency to downstream anabolic metabolism (Condon and Sabatini, 2019; Sabatini, 2017). Consistent with a role for mTORC1 in pDC activation, glycolysis has been reported to be increased in pDCs activated by TLR agonists and to be important for cytokine production (Bajwa et al., 2016; Wu et al., 2016).

Here, we hypothesized that a major function of IL-3R ligation in human pDCs is to synergize with TLRs to allow mTORC1 activation and the associated metabolic changes necessary for cellular activation. We discovered a critical role for IL-3- or GM-CSF-induced JAK2-STAT5 signaling in the expression of functional system L amino acid (LAA) transporters SLC7A5 (also known as LAT1, large neutral amino acid [LNAA] transporter 1) and SLC3A2. System LAA transport was obligatory for establishment of mTORC1 activity necessary for cytokine and chemokine production in response to a range of TLR agonists. We found that cytokine and chemokine production was restricted to a subset of pDCs in which mTORC1 was active and that this population of cells was transcriptionally similar to pDCs at the site of nephritic disease in SLE patients. *SLC7A11* (a subunit of cystine-glutamate transporter, $x_c^-$), ectonucleotide pyrophosphatase-phosphodiesterase 2 (*ENPP2*; which encodes autotaxin), and *MYO1E* (which encodes a non-muscle myosin) were the only differentially expressed genes shared between the cytokine producing clusters of pDCs activated by CpG-A *in vitro* and pDCs at sites of SLE-associated pathology. We found that small molecule inhibitors of $x_c^-$ and of ENPP2 were able to diminish cytokine production. Moreover, the combination of $x_c^-$ and JAK2 inhibitors effectively switched off cytokine production by activated pDCs. These data provide a mechanistic basis for inhibiting pDC activation through combinatorial targeting of amino acid transporters, a process which holds promise for treating diseases in which pDCs are implicated.

## RESULTS

### IL-3 primes pDCs for mTORC1 activation in response to TLR stimulation

Previous work has shown that production of type-I IFNs by pDCs in response to TLR ligands (Lande et al., 2007) is mTORC1-dependent (Cao et al., 2008). To explore this in more detail, we measured cytokine production over time by culturing pDCs from healthy donors (HDs) in medium containing IL-3 with or without CpG-A, a TLR9 agonist. Maximal IFN-α secretion occurred between 10 h and 12 h post activation, during which time ~50% of the cells made this cytokine (Figure S1A). Stimulation also resulted in TNF production, which peaked at 8 h, and declined rapidly thereafter (Figure S1A). Production of both cytokines ceased by ~24 h post activation (Figure S1A). Stimulation with CpG-A and other pDC-activating TLR agonists (TLR9: CpG-B and CpG-C; TLR7: resiquimod [R848] and imiquimod [R837]) also induced the expression of proinflammatory and homeostatic chemokines (Figure S1B).

To examine the role of IL-3 in pDC metabolism and function, we maintained pDCs overnight in medium with or without IL-3, after which we either left them untreated or stimulated with CpG-A (Figure S1C). We found that cell death was increased in the absence of IL-3 (Figure 1A) and that the addition of CpG-A was unable to rescue viability (Figure S1D). The absence of IL-3 had a marked inhibitory effect on CpG-A-induced IFN-α and TNF production (Figure 1B). This was not a reflection of cell death in the absence of IL-3, since cytokine measurements were made only in living cells. IL-3 was required for the CpG-A-induced transcription and translation of IFN-α (Figure 1C). However, IL-3 alone was sufficient to drive *TNF* transcription, but this mRNA was translated only following stimulation with CpG-A (Figure 1D). We found that the addition of other TLR9 or TLR7 agonists in the absence of IL-3 also led to increased cell death (Figures S1E and S1F) and diminished IFN-α and TNF production compared to when pDCs were cultured with IL-3 (Figures 1E and 1F).

Early work revealed that IL-3 acts as a growth factor to enhance anabolic pathways (Bauer et al., 2004; Vander Heiden et al., 2001). Since anabolism is controlled centrally by mTORC1 (Valvezan and Manning, 2019) and mTORC1 is important for pDC activation (Cao et al., 2008), we asked whether mTORC1 activity in pDCs is regulated by IL-3 by measuring phosphorylation of Ser235/236 of the ribosomal protein S6 (pS6), which

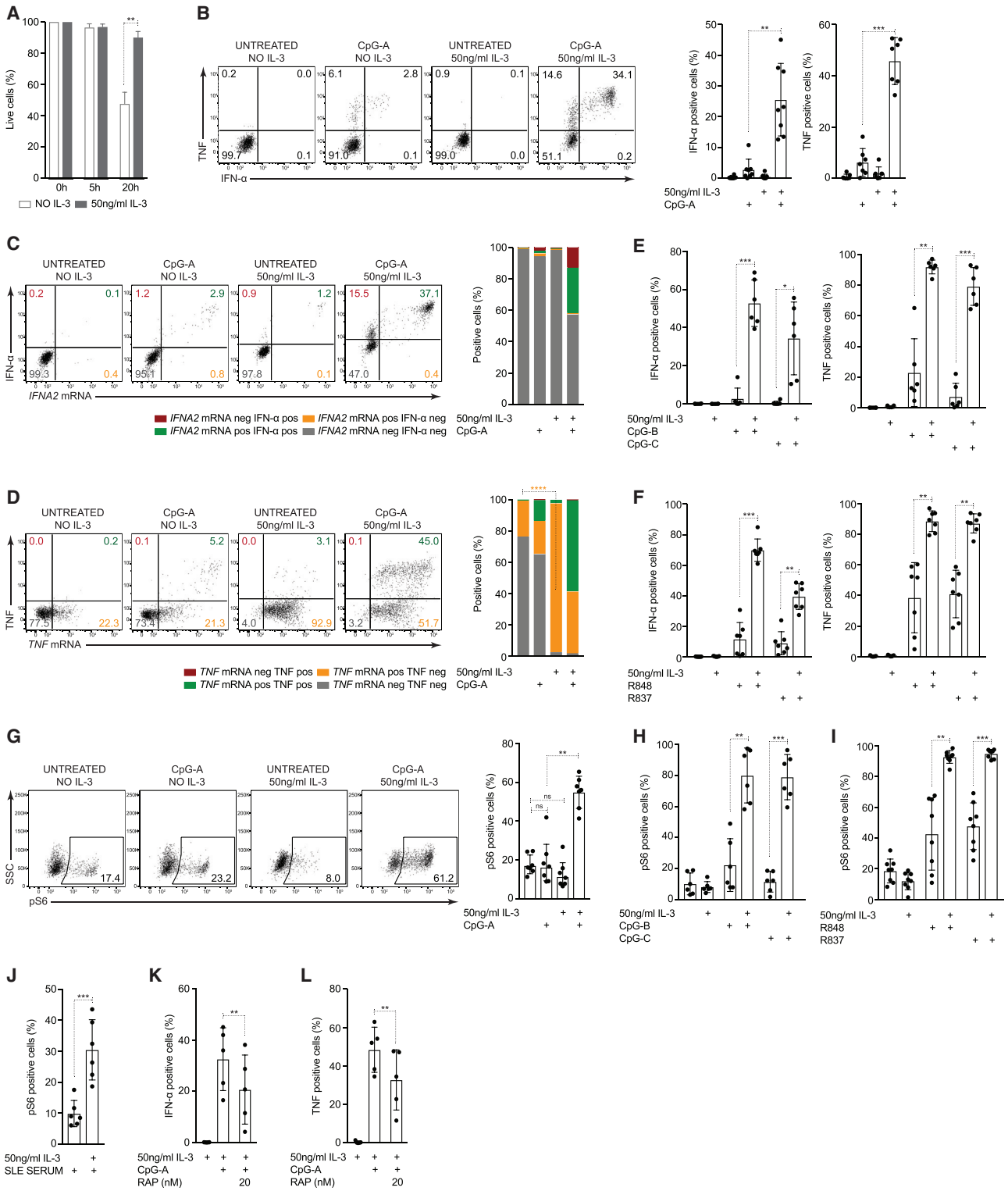


**Figure 1. IL-3 primes activated pDC for cytokine production and mTORC1 activation**

(A) Isolated pDCs were maintained in ± IL-3 media for indicated time and probed for live cells (n = 4 in 2 experiments).

(B–I, K, and L) Isolated pDCs maintained ± IL-3 and indicated inhibitors overnight (o/n) then stimulated ± indicated TLRs agonists for 5 h were probed for: (B, E, F, K, and L) IFN-α or TNF production (B, IFN-α: n = 8 in 5 experiments and TNF: n = 7 in 4 experiments; E, n = 6 in 2 experiments; F, n = 7 in 3 experiments; K and L, n = 5 in 4 experiments); (C) *IFNA2* mRNA expression and IFN-α production (n = 3 in 3 experiments); (D) *TNF* mRNA expression and TNF production (n = 3 in 3 experiments); and (G, H, I) pS6 expression (G, n = 7 in 4 experiments; H, n = 6 in 2 experiments; I, n = 8 in 3 experiments).

*(legend continued on next page)*

provides a measure of p70S6K activation, a direct mTORC1 target (Chauvin et al., 2014). We found pS6 in <20% of pDCs maintained without IL-3, and this was not increased by stimulation with CpG-A (Figure 1G). Maintenance in IL-3 alone did not increase pS6, but the combination of IL-3 followed by stimulation with CpG-A resulted in ~60% of pDCs becoming positive for pS6 (Figure 1G). Similarly, pDCs maintained in IL-3 and stimulated with CpG-B or CpG-C (Figure 1H) and R848 or R837 (Figure 1I) had higher frequencies of pS6-positive cells compared to their IL-3 deprived counterparts. Moreover, sera from SLE patients, which have been shown to activate pDCs, presumably due to the presence of DNA-containing immune complexes (Dzionek et al., 2001), also required IL-3 for induction of pS6 (Figure 1J) and sustaining cell viability (Figure S1G).

We then examined the effect of rapamycin (RAP), a selective mTORC1 inhibitor (Loewith et al., 2002), on activation-induced S6 phosphorylation and found that it limited the size of the pS6-positive population (Figure S1H). Therefore, IL-3 played a role in priming pDCs to allow mTORC1 activation upon TLR stimulation. Since pDCs were unable to make cytokines in response to CpG-A and other TLR agonists in the absence of IL-3, we reasoned that this could reflect the role of IL-3 in mTORC1 priming. Consistent with this, we confirmed findings that RAP-mediated inhibition of S6 phosphorylation was associated with inhibition of production of IFN-$\alpha$ (Figure 1K) (Cao et al., 2008) but also TNF (Figure 1L) by CpG-A-stimulated pDCs.

## mTORC1 primes pDCs for metabolic changes critical for activation

mTORC1 controls protein synthesis (Thoreen et al., 2012). To test if mTORC1 is driving translation in activated pDCs, we measured the incorporation of a puromycin analog into newly translated protein. Addition of CpG-A resulted in a significant increase in translation that was prevented by treatment with RAP or torin 1 (TOR) (Figure 2A; Figure S2A), which inhibits RAP-resistant functions of mTORC1 (Thoreen et al., 2009). Both inhibitors were almost as effective as the translation inhibitor cycloheximide (CXH) at blocking translation in activated pDCs (Figure 2A; Figure S2A).

mTORC1 is recognized to promote anabolic metabolism linked to increased glycolysis (Valvezan and Manning, 2019). Consistent with this, activated pDCs consumed more glucose than resting cells (Figure S2B). Moreover, the extracellular acidification rate (ECAR), a mark of lactate production, was increased in activated versus unstimulated pDCs (Figures 2B and 2C). Increased ECAR was linked to release of lactate (Figure 2D), was glucose-dependent (Figure 2B), and occurred within minutes after the addition of CpG-A (Figure 2C). Elevated ECAR persisted for at least 10 h, in line with the time course of cytokine production and mTORC1 activity. Tracing of carbon from $^{13}$C-labeled glucose supported the view that stimulation with CpG-A led to increased incorporation of glucose carbon into lactate but also revealed increased incorporation into tricarboxylic acid (TCA) cycle intermediates (Figure 2E). Consistent with the latter, the mitochondrial oxygen consumption rate (OCR), a mark of mitochondrial oxidative phosphorylation, was also increased in CpG-A-stimulated pDC (Figure S2C).

These findings indicated that metabolic changes occur early after pDC activation. To explore the role of increased glucose usage in pDC biology, we incubated CpG-A-stimulated cells with heptelidic acid (HPA), a selective inhibitor of glyceraldehyde-3-phosphate dehydrogenase (Endo et al., 1985), the central enzyme in the glycolysis pathway. HPA reduced lactate secretion (Figure 2F) and caused reductions in overall protein synthesis (Figure 2G) and production of IFN-$\alpha$ and TNF (Figure 2H) in the absence of any effects on viability (not shown). Inhibition of mTORC1 resulted in a decline in CpG-A-induced lactate release (Figure 2I), supporting a link between stimulation-dependent mTORC1 activation and increased glycolysis. We also found that the ATP synthase inhibitor oligomycin (OLI) (Lardy et al., 1958) inhibited IFN-$\alpha$ production similarly to HPA (Figure S2D) but had no effect on either TNF (Figure S2D) or viability (not shown). HPA and OLI combined inhibited IFN-$\alpha$ and TNF production completely (Figure S2D) and resulted in partial cell death (not shown). Taken together, these data indicate that stimulation with CpG-A in pDCs primed by exposure to IL-3 leads to an mTORC1-dependent increase in glucose metabolism that is critical for pDC activation.

## IL-3 induces the expression of SLC7A5 and SLC3A2 that permit mTORC1 activation in response to TLR stimulation

mTORC1 activation depends on the presence of sufficient environmental amounts of amino acids, among which leucine and methionine are of particular importance (Condon and Sabatini, 2019; Valvezan and Manning, 2019). In T cells, both of these amino acids are acquired from the environment via system LAA transporters, which comprise a heterodimer of the solute carriers, catalytic SLC7A5, and multifunctional protein SLC3A2 (CD98) (Sinclair et al., 2019; Sinclair et al., 2013). Other system LAA transporters are composed of SLC7A6, SLC7A7, or SLC7A8 paired with SLC3A2 (Verrey et al., 2004). Single-cell RNA sequencing (scRNA-seq) revealed that the majority of pDCs maintained in IL-3 expressed *SLC7A5* regardless of CpG-A stimulation (Figure S3A). *SLC7A6* expression was limited (Figure S3A), and *SLC7A7* and *SLC7A8* transcripts were not detected. *SLC7A5* and *SLC3A2* transcripts were co-expressed in the majority of pDCs cultured in IL-3 and stimulated with CpG-A (Figure 3A). This was a result of the signal delivered by IL-3, since ~97% of pDCs cultured in IL-3 but not stimulated with CpG-A were also positive for *SLC7A5* and *SLC3A2* transcripts. In contrast, significantly fewer cells maintained without IL-3 expressed these solute carriers, and stimulation with CpG-A did not rescue their expression (Figure 3A).

To assess whether IL-3-induced expression of *SLC7A5* and *SLC3A2* allowed the assembly of a functional system LAA

(J) Isolated pDCs maintained in IL-3 with no fetal bovine serum (FBS) o/n were stimulated with SLE sera (1:2) for 10 h and probed for pS6 expression (n = 6 in 1 experiment).

Representative plots from individual donors (n, see above) are shown (B–D and G). Bar graphs are shown as (A, B, and E–L) mean ± SD and (C and D) mean. Dots represent individual donors (n).

Please also see Figure S1.

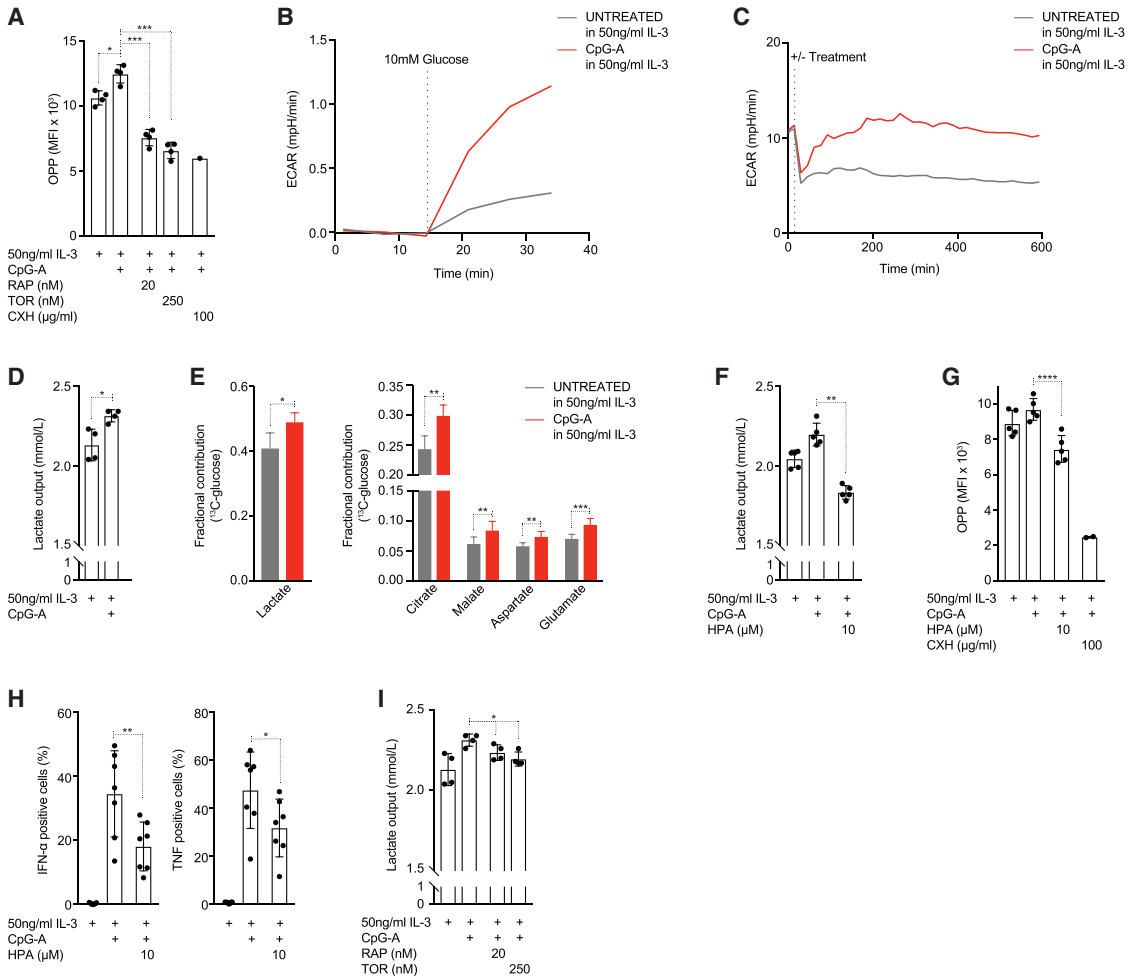


**Figure 2. pDC activation is coupled to mTORC1 activity and changes in metabolism**

Isolated pDC maintained in IL-3 were probed for:

(A and G) Protein synthesis measured by incorporation of puromycin analog (OPP) in cells stimulated ± CpG-A for 10 h and indicated inhibitors (A, n = 4 in 1 experiment; G, n = 5 in 2 experiments).

(B) ECAR before and after addition of glucose in cells stimulated ± CpG-A for 5 h after o/n rest (representative of n = 3 in 2 experiments).

(C) Baseline ECAR measured by mitochondrial stress test in cells stimulated ± CpG-A (mean from n = 7 in 6 experiments).

(D, F, and I) Lactate concentration in media from cells stimulated ± CpG-A and ± indicated inhibitors for 10 h (D and I, n = 4 in 1 experiment, untreated and CpG-A-treated conditions shared between experiments; F, n = 5 in 2 experiments).

(E) Indicated metabolites shown as fractional contribution of newly synthesized $^{13}$C-glucose carbon-incorporation after 3 h stimulation ± CpG-A (n = 5 in 2 experiments).

(H) IFN-α or TNF production, where indicated cells were pre-treated with inhibitor o/n and then stimulated ± CpG-A for 5 h (n = 7 in 4 experiments).

Bar graphs are shown as (A and D–I) mean ± SD. Dots represent individual donors (n).

Please also see Figure S2.

transporter, we measured the uptake of kynurenine, a naturally fluorescing molecule that is transported into cells via SLC7A5; this can be used as a proxy measurement of LNAA uptake (Sinclair et al., 2018). The ability of pDCs to take up kynurenine aligned with their expression of *SLC7A5* and *SLC3A2* and pinpointed IL-3 as conferring this capability (Figure 3B; Figure S3B). Addition of BCH, a system LAA transporter-specific inhibitor (Sinclair et al., 2013), abrogated transport of kynurenine, confirming that uptake was SLC7A5-dependent (Figure 3B; Figure S3B). Of interest, freshly isolated pDCs from SLE patients and HDs also expressed *SLC7A5* and *SLC3A2* (Figure S3C), and furthermore, HD pDCs had the ability to take up kynurenine immediately *ex vivo*, a process that was blocked by BCH (Figure S3D).

To confirm that functional system LAA transport was a prerequisite for mTORC1 activation in response to CpG-A, we examined the effects of IL-3 and CpG-A on combined measurements of kynurenine uptake, S6 phosphorylation, and cytokine production. This revealed that in the absence of IL-3, most pDCs were negative for kynurenine transport and pS6 (Figure 3C). Stimulation with CpG-A resulted in a slight increase in pS6-positive cells that were able to take up kynurenine (Figure 3C). As expected,

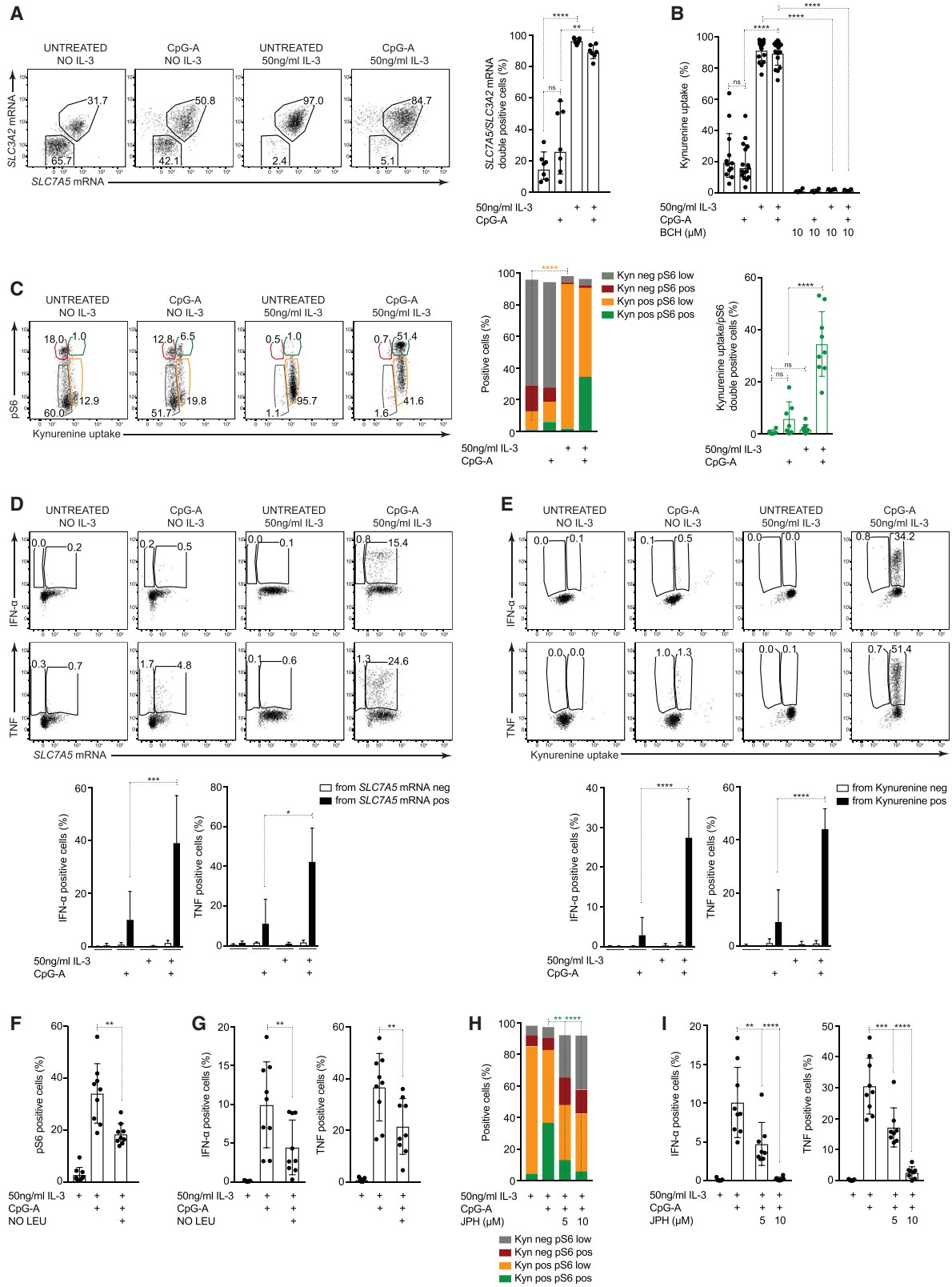


**Figure 3. IL-3 induces the expression of functional system LAA transporters that license mTORC1 activation**

(A–E) Isolated pDCs maintained ± IL-3 o/n then stimulated ± CpG-A for 5 h were probed for: (A) *SLC7A5* and *SLC3A2* mRNA expression (n = 7 in 4 experiments); (B) kynurenine uptake (n = 13–18 in 9 experiments); (C) kynurenine uptake and pS6 expression (n = 7–9 in 5-6 experiments); (D) *SLC7A5* mRNA expression and

*(legend continued on next page)*

maintenance in IL-3 allowed the majority of pDCs to take up kynurenine (Figure 3C), but these cells remained negative for pS6. However, addition of CpG-A led to the emergence of a significant population of kynurenine and pS6 double-positive cells (Figure 3C), in which S6 phosphorylation, but not kynurenine uptake, was inhibited by RAP (Figure S3E). Stimulation with other TLR agonists in the presence of IL-3 also led to an increase in pS6-positive cells capable of taking up kynurenine (Figure S3F). Moreover, IFN-$\alpha$ and TNF production occurred only in cells that expressed *SLC7A5* (Figure 3D) and were therefore able to take up kynurenine (Figure 3E).

To confirm the role of system LAA transport in pDC activation, we cultured cells in leucine- or methionine-free media and found that phosphorylation of S6 and cytokine production were dependent on added leucine (Figures 3F, G) but not methionine (Figures S3G and S3H). Further, cells in which *SLC3A2* or *SLC7A5* were deleted using CRISPR (Figures S3I and S3J) had diminished capacity to produce IFN-$\alpha$ and TNF (Figures S3K and S3L). Consistent with this, the SLC7A5-specific inhibitor JPH203 (Oda et al., 2010) caused a marked dose-dependent reduction in pDCs that were positive for both pS6 and kynurenine uptake (Figure 3H) and IFN-$\alpha$ and TNF production (Figure 3I). These data show that IL-3 is essential for the induction of the system LAA transporters *SLC7A5* and *SLC3A2* in pDCs and that uptake of leucine, mediated by these transporters, is necessary for priming subsequent activation of mTORC1 and cytokine production by pDCs in response to TLR agonists.

### Inhibition of JAK2-dependent signaling downstream of IL-3R prevents mTORC1 activation and cytokine and chemokine production in response to TLR stimulation

The common $\beta_c$ (encoded by *CSF2RB*) of the IL-3R couples signals from IL-3 to the JAK2-STAT5 pathway (Mui et al., 1995; Reddy et al., 2000). Using published data examining STAT5 chromatin immunoprecipitation sequencing in human $CD4^+$ T cells (Schmidl et al., 2014), we found STAT5 DNA binding sites in *SLC7A5* and *SLC3A2* loci (Figure S4A), suggesting that the JAK2-STAT5 pathway could be responsible for the IL-3 induced expression of these genes. Moreover, IL-3, but not CpG-A, was able to induce phosphorylation of STAT5 (Y694, pSTAT5) (Figure 4A). Therefore, we examined the effects of the selective JAK2 inhibitor AZD1480 (AZD) (Ioannidis et al., 2011) and the clinically used JAK1 and 2 inhibitor baricitinib (BAR) (Markham, 2017) on CpG-A-induced activation in pDCs cultured in IL-3. We examined BAR because a recent randomized, placebo-controlled phase 2 clinical trial showed that it significantly reduced disease activity in SLE patients (Wallace et al., 2018). AZD and BAR inhibited STAT5 phosphorylation (Figure 4A), *SLC7A5* and *SLC3A2* expression (Figure 4B), kynurenine uptake (Figure 4C), and the phosphorylation of S6 (Figure 4D). Further, JAK2 inhibition resulted in marked reduction in IFN-$\alpha$ and TNF production linked to reduced ability to take up kynurenine (Figure 4E). Looking at the intersection between kynurenine transport and mTORC1 activity, we found that JAK2 inhibition resulted in the loss of cells that were positive for both processes (Figure 4F), which was a similar outcome to that observed in IL-3-deprived cells (Figure 3C). Finally, we observed that only pDCs with both high rates of kynurenine uptake and high mTORC1 activity made IFN-$\alpha$ (Figure 4G; Figure S4B) and that cytokine production was lost following JAK2 inhibition (Figure 4G).

As was the case for IFN-$\alpha$, priming with IL-3 was necessary for maximal chemokine production in response to CpG-A (Figure S4C). The majority of *CCL3*-, *CCL17*-, and *CXCL10*-positive cells co-expressed *IFNA2*, while only a portion of the *CXCL8*- and *CXCL9*-positive cells concomitantly expressed *IFNA2* (Figure S4C). Absence of IL-3 priming prior to stimulation with CpG-A resulted in diminished chemokine and *IFNA2* double-positive populations (Figure S4C). This was likely the result of diminished JAK2-mediated signaling, since AZD and BAR treatment also resulted in loss of pDC double positive for *IFNA2* and chemokine transcripts (Figure S4C).

Since system LAA transporters were expressed in pDCs circulating in HD blood (Figure S3C), and their expression could be repressed by JAK2 inhibitors *in vitro* (Figure 4B), we examined expression of *SLC7A5* and *SLC3A2* in pDCs from rheumatoid arthritis (RA) patients treated with tofacitinib (TOF) (Conaghan et al., 2016), a pan-JAK inhibitor (Boor et al., 2017). For comparison, we used pDCs from HDs and from RA patients treated with rituximab (RIT, a B cell-depleting antibody [Ab]). We validated that TOF inhibited *SLC7A5* and *SLC3A2* expression (Figure S4D) and IFN-$\alpha$ and TNF production (Figure S4E) in pDCs stimulated with IL-3 plus CpG-A *in vitro*. Consistent with this, *SLC7A5*- and *SLC3A2*-positive pDCs were less frequent in TOF-treated RA patients than in HDs or RIT-treated RA patients (Figure 4H; Figure S4F). *SLC7A5* and *SLC3A2* expression in pDCs from RIT-treated RA patients versus HDs was similar (Figure 4H; Figure S4F). It is plausible then that JAK2-regulated expression of system LAA transporters *in vivo* is responsible for modulating the production of cytokines in pDC-driven pathologies.

The fact that *ex vivo*-isolated pDCs expressed *SLC7A5* and *SLC3A2* and were able to take up kynurenine (Figures S3C and S3D) correlated with their ability to respond to CpG-A by making cytokines and chemokines even in the absence of added IL-3 (Figure S4G). Nevertheless, pDC activation in this setting was still inhibited by AZD and BAR (Figure S4G), indicating that the cells retained a functional memory of signaling initiated *in vivo* by the common $\beta_c$ of the IL-3 receptor.

IFN-$\alpha$ or TNF production (IFN-$\alpha$: n = 6 in 4 experiments and TNF: n = 3 in 2 experiments); (E) kynurenine uptake and IFN-$\alpha$ or TNF production (IFN-$\alpha$: n = 5–7 and TNF: n = 6–7 in 5 experiments); and (A–C and E) CpG-A condition shared with Figures 4B–4F.

(F and G) Isolated pDCs maintained in regular or leucine-free media plus IL-3 o/n then stimulated ± CpG-A for 5 h were probed for: (F) pS6 expression and (G) IFN-$\alpha$ or TNF production, untreated and CpG-A conditions shared with Figures 6D, 6F, S3G, and S3H (F and G, n = 9 in 3 experiments).

(H and I) Isolated pDCs maintained with IL-3 ± JPH203 o/n then stimulated ± CpG-A for 5 h were probed for: (H) kynurenine uptake and pS6 expression and (I) IFN-$\alpha$ or TNF production (H and I, n = 8–9 in 3 experiments).

Representative plots from individual donors (n, see above) are shown (A, C, D, and E). Bar graphs are shown as (A and B) geometric mean ± geometric SD, (C–G and I) mean ± SD, and (C and H) mean. Dots represent individual donors (n).

Please also see Figure S3.

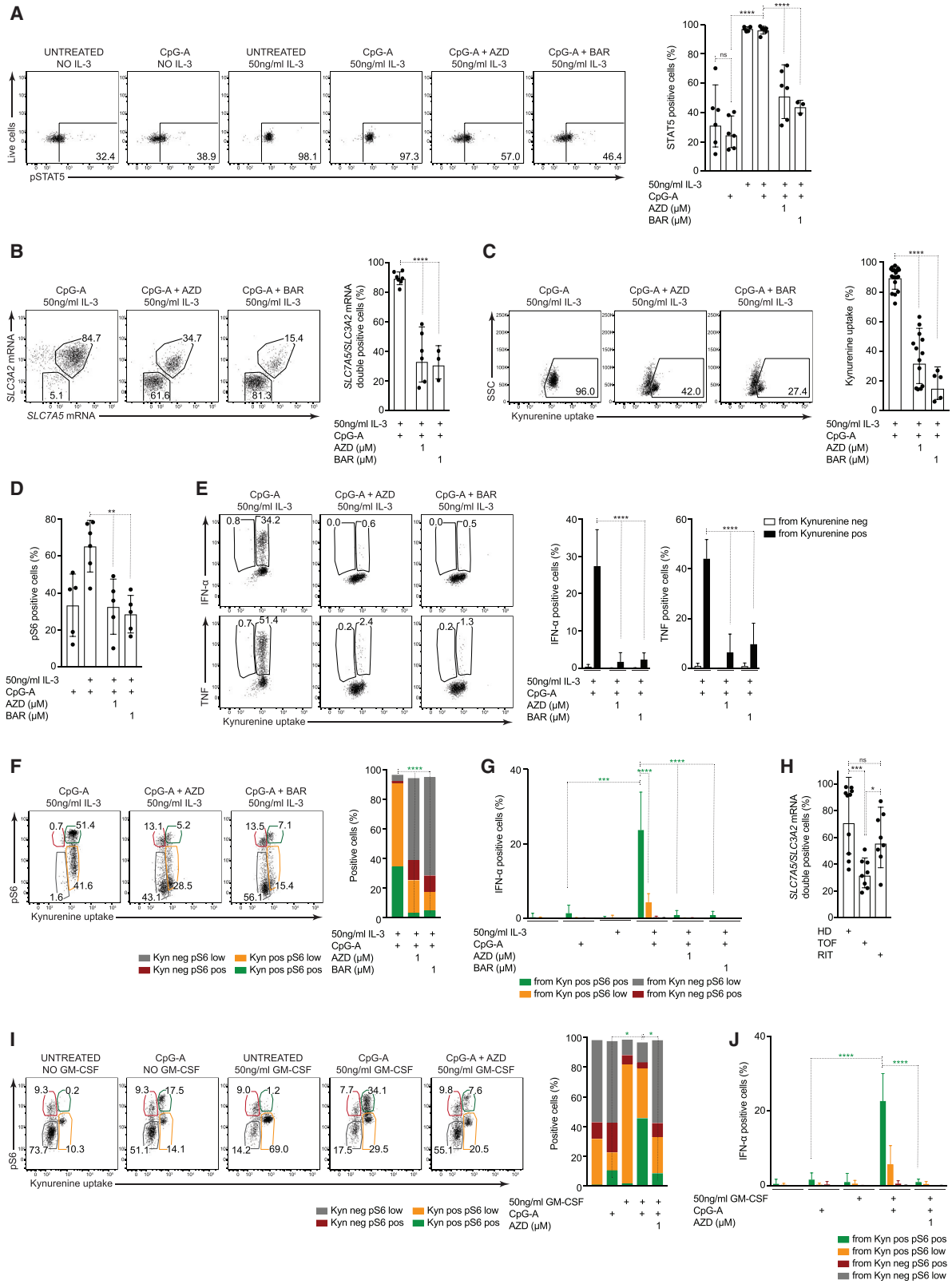


**Figure 4. Inhibition of JAK2 prevents mTORC1 activation and cytokine production**

(A–G) Isolated pDCs maintained ± IL-3 and indicated inhibitors o/n then stimulated ± CpG-A for 5 h were probed for: (A) pSTAT5 (Y694) expression (n = 3–6 in 2–3 experiments); (B) *SLC7A5* and *SLC3A2* mRNA expression (n = 3–6 in 2 experiments); (C) kynurenine uptake (n = 5–13 donors in 3–6 experiments); (D) pS6

*(legend continued on next page)*

The common $\beta_c$ of the IL-3R is also the signaling component of the GM-CSF and IL-5 receptors (Dougan et al., 2019). Human pDCs express GM-CSFR$\alpha$ (encoded by *CSF2RA*) as well as IL-3R$\alpha$ (Figure S4H) but do not express IL-5R$\alpha$ (Ghirelli et al., 2010). GM-CSF concentration can be elevated in sera from SLE patients (Willeke et al., 2004), and like IL-3, GM-CSF can promote pDC survival and IFN-$\alpha$ production following TLR7-stimulation *in vitro* (Leonard et al., 2016). We reasoned, therefore, that effects of GM-CSF on pDCs would recapitulate those of IL-3. We found that, like IL-3, GM-CSF supported pDC survival (Figure S4I) and induced a population of cells with high rates of kynurenine uptake and mTORC1 activity (Figure 4I) that produced IFN-$\alpha$ in response to CpG-A (Figure 4J). Moreover, all of these parameters were inhibited by AZD (Figures 4I and 4J).

Taken together, these data reveal the emergence of a subpopulation of pDCs capable of making cytokines and chemokines in response to TLR agonists. These cells express functional system LAA transporters and are able to activate mTORC1 upon exposure to CpG-A. These processes are dependent on priming by IL-3 or GM-CSF through the JAK2-STAT5 pathway downstream of the common $\beta_c$. The data highlight JAK2 as a therapeutic target in conditions where pDC activation is implicated in disease.

## TLR stimulation induces expression of SLC7A11, ENPP2, and MYO1E in type I IFNs producing pDCs

Even at peak cytokine production, only a subset of stimulated pDCs was positive for cytokine production and pS6 (Figures S1A and S1H). This led us to explore heterogeneity within the pDC population through scRNA-seq. We again used purified pDCs (Figure S5A) maintained in IL-3 and stimulated with or without CpG-A (Figure S1C). Individually sequenced cells aligned into 12 transcriptionally distinct clusters (Figure S5B). Of these, 1, C9, was apparent only after stimulation with CpG-A (Figure S5C). We found that the contributions of C2, C4, and C7 to the overall pDC population increased following stimulation with CpG-A (Figure S5D). Within these clusters, only C9 and C2 were enriched in type I IFN transcripts (Figure 5A). Despite the expected broad expression of *TNF*, C9 in particular was also enriched in TNF transcripts (Figure S5E). Likewise, C9 was enriched in expression of proinflammatory chemokines (Figure S5F). C2 and C9 had similar transcriptional profiles, evident by their proximity on the Uniform Manifold Approximation and Projection (UMAP) as well as in the clustering hierarchy (Figures S5C and S5G).

We compared transcriptomes from *in vitro*-activated pDCs with scRNA-seq data of pDCs isolated from lupus nephritis kidney biopsies (SLE pDCs) (Arazi et al., 2019). Consistent with our findings regarding the importance of IL-3- or GM-CSF-initiated signaling and system LAA transporter expression for pDC activation, we found that SLE pDCs (C22) expressed *IL3RA, CSF2RA, CSF2RB, SLC3A2*, and *SLC7A5* (Figure 5B). Indeed, expression of these genes within the immune cell populations of nephritic kidney biopsies was highest in pDCs (C22) (Figure 5B). Next, we identified genes differentially expressed in C2 and C9 from *in vitro*-activated pDCs and in SLE pDCs compared to all other clusters in their respective datasets using UpSet (Conway et al., 2017). Our analysis showed that of the 43 unrelated genes shared between C9, C2, and SLE pDCs (Figure 5C), 21 were differentially regulated in C2 or C9 (Figure S5H), with expression of *SLC7A11* increased in both clusters. Moreover, *SLC7A11*, together with *ENPP2* and *MYO1E*, constituted a set of 3 genes co-expressed by all 3 groups of cells (Figure 5C) and not included in any other cluster. These genes were enriched in the type I IFN- and TNF-producing C9, and to a lesser degree C2 (Figure 5D; Figure S5I), and a large percentage of the cells within these clusters expressed the genes (Figure 5E). Moreover, among lesional immune cell populations from lupus nephritis kidney biopsies, *SLC7A11* and *ENPP2* were expressed almost exclusively in SLE pDCs (C22), while *MYO1E* was also expressed by 2 non-pDC clusters (Figure 5F). RNA-flow analysis confirmed that *SLC7A11*, *ENPP2*, and *MYO1E* were expressed when pDCs were stimulated with CpG-A and with other TLR agonists (Figure S5J). The majority of cells expressing these genes co-expressed *IFNA2* when stimulated with CpG-A (Figure S5K).

We reasoned that if expression of *SLC7A11, ENPP2*, and *MYO1E* marked type I IFN- and TNF-producing pDCs, expression of these genes should be detectable in pDCs in other pathological sites in which pDC infiltration is implicated in disease. We explored this for SLC7A11 by staining sections from diseased skin from patients with cutaneous lupus with antibodies against SLC7A11 and the IL-3R$\alpha$. The analysis revealed an increase in SLC7A11-positive cells in the skin of cutaneous lupus patients compared to skin from HDs (Figure S5L). Most of these cells were IL-3R$\alpha$-positive, although other, currently unidentified, cells also expressed SLC7A11 (Figure S5M). Moreover, we found no evidence for *SLC7A11* expression in circulating pDCs from HDs or SLE patients (SLEDAI [Lam and Petri, 2005] from 0 to 8) (Figure S5N) or of *ENPP2* or *MYO1E* expression in *ex vivo* pDCs from HDs (Figure S5O). Together, these data suggest that *SLC7A11*, *ENPP2*, and *MYO1E* expression are marks of activated, cytokine-producing tissue-residing pDCs.

Unlike *SLC7A5* and *SLC3A2* (Figure S3C), *SLC7A11*, *ENPP2*, and *MYO1E* (Figures S5N and S5O) were not expressed by circulating pDCs, and hence, we reasoned their expression was not regulated by the common $\beta_c$. This was confirmed for *SLC7A11* when we found that IL-3 alone was incapable of inducing expression of this gene (Figures 5G and 5H). Rather, *SLC7A11* was

expression (n = 5–6 in 4 experiments); (E) kynurenine uptake and IFN-$\alpha$ (n = 3 in 2 experiments) or TNF production (n = 2–3 in 1–2 experiments]; (F) kynurenine uptake and pS6 expression (n = 5 in 3 experiments); (B–F) CpG-A condition shared with Figures 3A–3C and 3E; and (G) IFN-$\alpha$ production (n = 4–5 in 2–3 experiments).

(H) Isolated pDCs from HDs and RA patients treated with TOF or RIT were probed for *SLC7A5* and *SLC3A2* mRNA expression (n = 8–10 in 2 experiments).

(I and J) Isolated pDCs maintained ± GM-CSF and indicated inhibitors o/n then stimulated ± CpG-A for 5 h were probed for: (I) kynurenine uptake and pS6 expression and (J) IFN-$\alpha$ production (I and J, n = 4 in 2 experiments).

Representative plots from individual donors (n, see above) are shown (A–C, E, F, and I). Bar graphs are shown as (A–C and H) geometric mean ± geometric SD, (D, E, G, and J), mean ± SD, and (F and I) mean. Dots represent individual donors (n).

Please also see Figure S4.

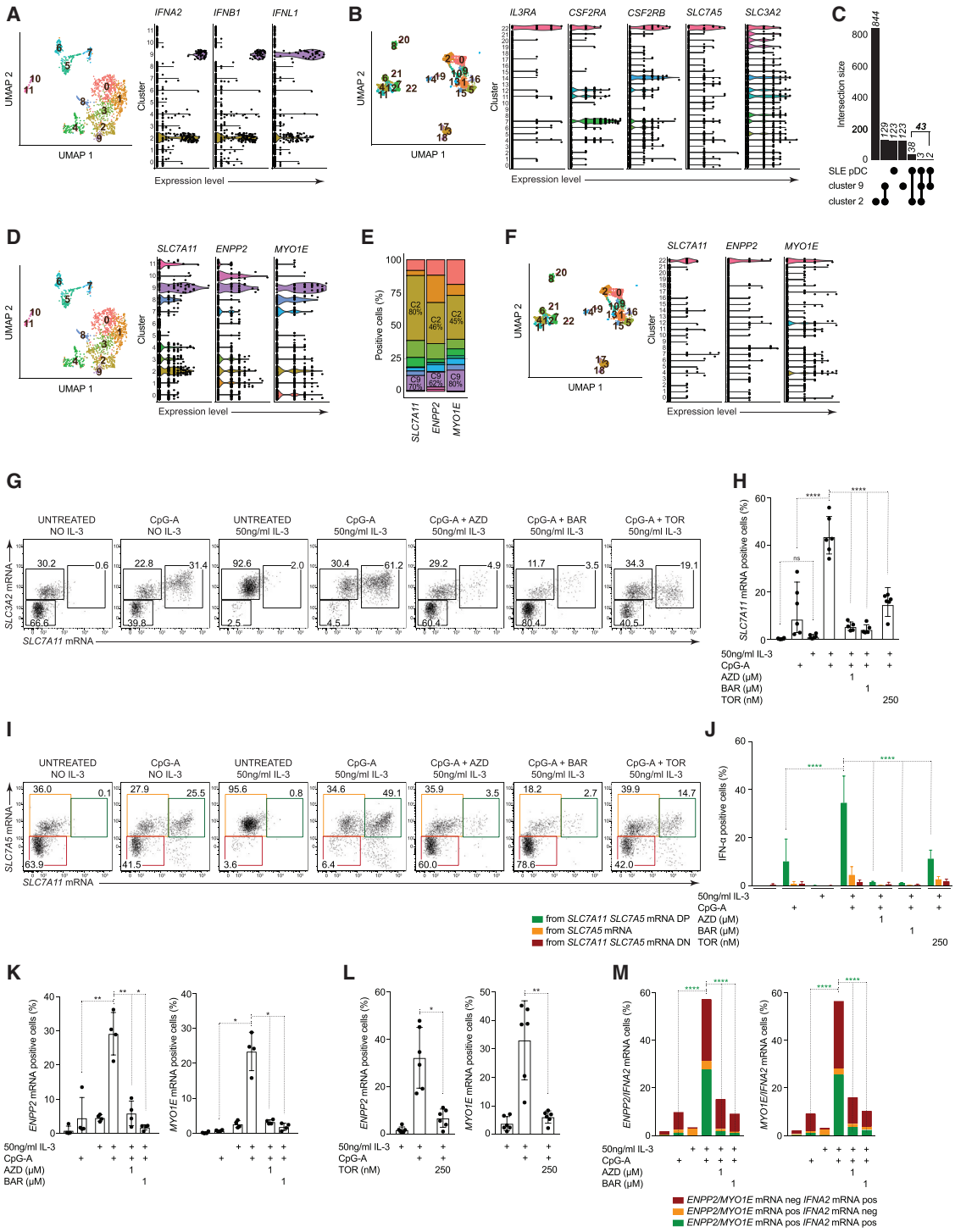


**Figure 5. Activated pDCs express SLC7A11, ENPP2, and MYO1E**

(A, D, and E) Isolated pDCs maintained in IL-3 o/n then stimulated ± CpG-A for 5 h (*in vitro* pDCs) were subjected for scRNA-seq analysis presented as UMAP plot colored by clusters and violin plot of (A) *IFNA2*, *IFNB1*, and *IFNL1* and (D) *SLC7A11*, *ENPP2*, and *MYO1E* expression across clusters; (E) bar graph with indicated frequencies of *SLC7A11*, *ENPP2*, and *MYO1E* expression within C2 and C9 in *in vitro* pDCs (A, D, and E, n = 1 in 1 experiment).

(B and F) Re-analyzed scRNA-seq data of pDCs (SLE pDCs) and other immune cells from kidney biopsies of lupus nephritis patients (Arazi et al., 2019) presented as UMAP plot colored by clusters and violin plots of (B) *IL3RA*, *CSF2RA*, *CSF2RB*, *SLC7A5*, and *SLC3A2* and (F) *SLC7A11*, *ENPP2*, and *MYO1E* expression across clusters.

(C) Comparative analysis of differentially expressed genes from *in vitro* pDCs and *in* SLE pDCs (C22) presented as UpSet plot with the intersection of differentially expressed genes between pDCs and SLE pDCs.

*(legend continued on next page)*

expressed in response to stimulation with CpG-A (Figures 5G and 5H). *SLC7A11* encodes the specific subunit of $x_c^-$, which, when chaperoned by SLC3A2, allows cells to take up cystine in exchange for glutamate (Bassi et al., 2001). Expression of *SLC7A11* was coupled to expression of *SLC3A2* (Figure 5G), indicating that activated pDCs can express functional $x_c^-$ transporter. While IL-3 alone was incapable of inducing *SLC7A11* expression, it was critical for priming cells to express *SLC7A11* in response to CpG-A, since JAK2 inhibition prevented this from happening (Figures 5G and 5H). This was likely the result of a requirement for IL-3-mediated system LAA transporter expression for optimal mTORC1 activation, because TOR (Figures 5G and 5H) and RAP (Figure S5Q) also inhibited *SLC7A11* expression. Consistent with this, pDCs maintained in IL-3 and stimulated with CpG-A had the highest frequencies of *SLC7A11* and *SLC7A5* double-positive cells (Figure 5I; Figure S5P), and as a result, produced IFN-α at full capacity (Figure 5J). In contrast, pDCs deprived of IL-3 or treated with AZD or BAR lost expression of both transporters and hence IFN-α production (Figures 5I and 5J; Figure S5P). Treatment with TOR had similar, although less pronounced effects than AZD and BAR (Figures 5I and 5J; Figure S5P).

As for *SLC7A11*, CpG-A-induced expression of *ENPP2* and *MYO1E* required priming of mTORC1 by IL-3, since it was inhibited by AZD, BAR (Figure 5K), TOR (Figure 5L) and RAP (Figure S5Q). Blunted *ENPP2* and *MYO1E* expression correlated with loss of *IFNA2* expression (Figure 5M). Together, these data indicate that expression of *SLC7A11*, *ENPP2*, and *MYO1E* correlate with type I IFN expression in activated pDCs.

## Coordinated inhibition of SLC7A11 and JAK2 potently blocks cytokine production by CpG-A-activated pDCs

The finding that *SLC7A11*, *ENPP2*, and *MYO1E* expression distinguished activated tissue-residing pDCs from circulating pDCs makes them attractive therapeutic targets. In this context, SLC7A11 is of particular interest since $x_c^-$ is a target of the anti-inflammatory drug sulfasalazine (SAZ) (Gout et al., 2001), which is in clinical use for the treatment of RA, ulcerative colitis, and Crohn's disease (Choi and Fenando, 2020). $x_c^-$ is also inhibited by erastin (ERA) (Dixon et al., 2014), which is able to suppress septic shock and inflammatory gene expression associated with lipopolysaccharide-activated macrophages (Oh et al., 2019). We found that both ERA and SAZ inhibited CpG-A-induced IFN-α and TNF production (Figure 6A). This was associated with reductions of cells that had high rates of both kynurenine uptake and S6 phosphorylation (Figure 6B; Figure S6A), which was consistent with the fact that only pDCs with both of these attributes made cytokine (Figure 6C). Inhibition occurred in the absence of appreciable cell death (Figure S6B). ERA and SAZ have been reported to have inhibitory effects on targets additional to $x_c^-$ (Chidley et al., 2011; Yagoda et al., 2007). Therefore, we directly tested the role of SLC7A11 using CRISPR to delete *SLC7A11* (Figure S6C) and, by using medium free of cystine, the substrate for $x_c^-$ (Figures 6D–6F), found that the effects were similar to those exerted by ERA and SAZ (Figures 6A–6C, Figure S6A), although there was less of an effect on kynurenine uptake in the absence of extracellular cystine than there was in the presence of the inhibitors (Figure S6D).

We found that ERA, SAZ (Figure 6G), or culture in cystine-free medium (Figure S6E) inhibited the expression of *ENPP2* and *MYO1E* in pDCs stimulated with IL-3 plus CpG-A, indicating that SLC7A11 could regulate both of these genes. We reasoned, therefore, that loss of pDC effector functions due to SLC7A11 inhibition could reflect loss of ENNP2 or MYO1E function. We addressed this possibility, focusing on *ENPP2*, elevated expression of which is found in various inflammatory and malignant conditions like fibrosis (Ninou et al., 2018) and systemic sclerosis (Castelino et al., 2016). We found that ziritaxestat (ZIR), an ENPP2 inhibitor (Desroy et al., 2017), inhibited the activation of pDCs by IL-3 plus CpG-A (Figures 6H and 6I; Figure S6F), suggesting that the importance of SLC7A11 in pDC activation is linked to its ability to regulate *ENPP2* expression.

Given the effectiveness of targeting JAK2 and $x_c^-$ in limiting cytokine production, we asked whether a combinatorial approach of inhibiting both JAK2 and $x_c^-$ might result in further loss of pDC function. We performed an *in vitro* dose escalation to define the effects of BAR on viability and cytokine production by activated pDCs. We found that production of IFN-α and TNF (Figure 6J) declined as the concentration of BAR rose from 25 to 100 nM and that this was accompanied by increased cell death (Figure S6G). Moreover, the doses of BAR and SAZ that alone were suboptimal synergized to increase the inhibition of both IFN-α and TNF production (Figure 6J) without diminishing cell survival beyond that seen with BAR alone (Figure S6G).

To more closely model the situation *in vivo*, we performed experiments in human plasma-like medium (HPLM), which reflects the composition of human plasma (Cantor et al., 2017). pDCs activated with CpG-A in HPLM showed dependency on IL-3-mediated mTORC1 activity for production of cytokines and only cells with high rates of kynurenine uptake and high pS6 (Figure 6K; Figure S6H) had the capacity to produce IFN-α and TNF (Figure 6L). Moreover, inhibition of JAK2, $x_c^-$, or ENPP2 (Figures 6H, 6I, 6K, 6L; Figures S6F and S6H), and of JAK2 and $x_c^-$ together (Figures 6K and 6L; Figure S6H), were able to block pDC activation in HPLM.

Together, our data indicate that pDC activation is associated with the expression of *SLC7A11* and, in an SLC7A11-dependent fashion, *ENPP2* and *MYOE1*. Inhibition of $x_c^-$ or ENPP2 is able to suppress the ability of pDCs to produce IFN-α and TNF. Furthermore, a combinatorial approach for suppressing pDC activation by targeting both JAK2 and $x_c^-$ results in an additive inhibitory effects that essentially prevents cytokine production.

(G–M) Isolated pDCs were maintained ± IL-3 and indicated inhibitors o/n then stimulated ± CpG-A for 5 h and probed for: (G) *SLC7A11* and *SLC3A2* mRNA expression; (H) *SLC7A11* mRNA expression; (I) *SLC7A11* and *SLC7A5* mRNA expression (G–I, n = 5–6 in 3 experiments); (J) IFN-α production (n = 3–4 in 2 experiments); (K and L) *ENPP2* or *MYO1E* mRNA expression; untreated and/or CpG-A conditions shared with Figures 6G and S5Q; and (M) *IFNA2* and *ENPP2* or *MYO1E* mRNA expression (K–M, n = 4 in 2 experiments).

Representative plots from individual donors (n, see above) are shown (G and I). Bar graphs are shown as (H) geometric mean ± geometric SD, (J–L) mean ± SD, and (M) mean. Dots represent individual donors (n).

Please also see Figure S5.

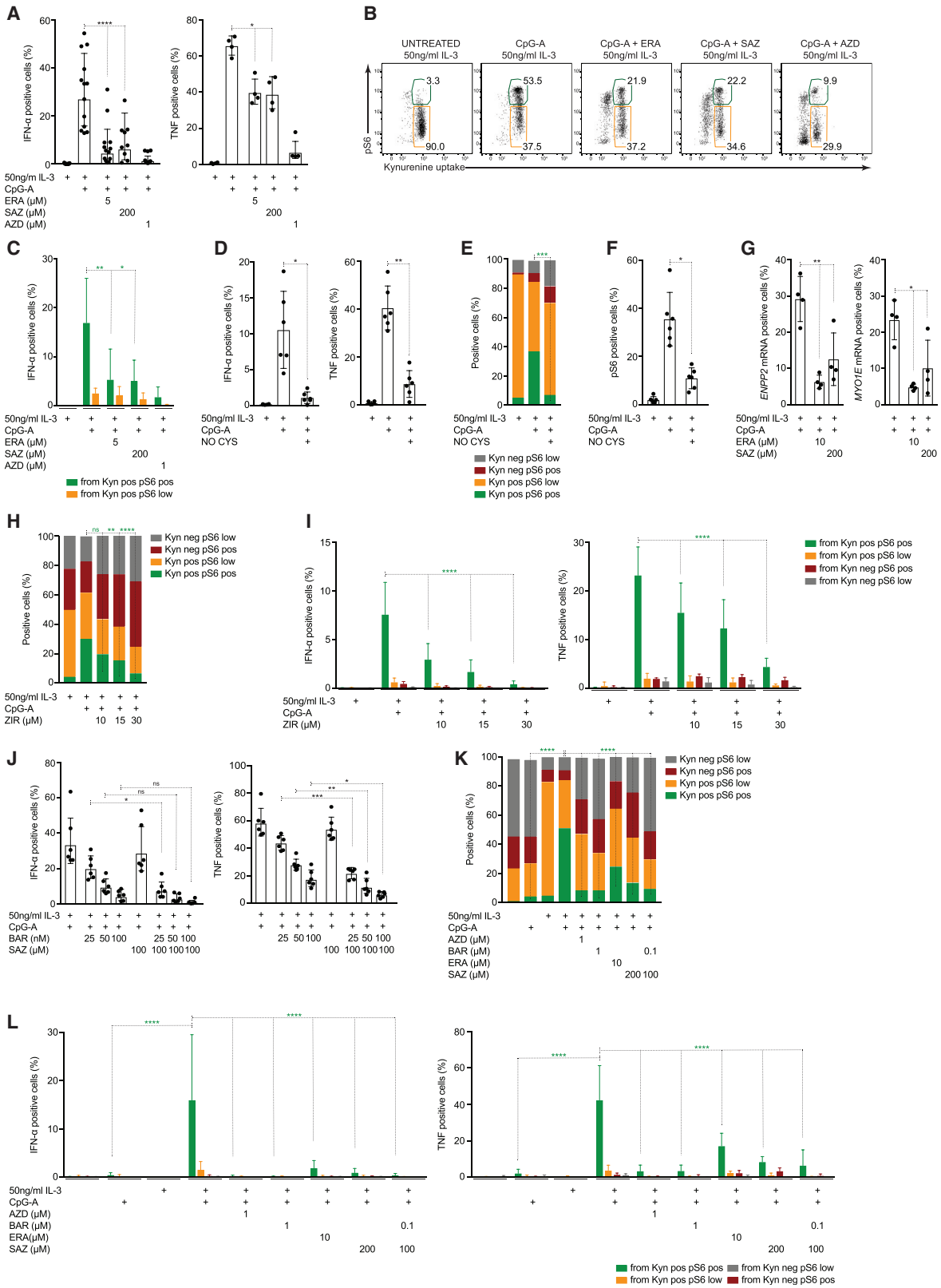


*(legend on next page)*

## DISCUSSION

Our initial observations that IL-3 or GM-CSF were not only important for pDC survival but also primed pDCs for subsequent activation prompted us to explore the causality between IL-3 or GM-CSF and IFN-α and TNF production. IL-3 has been shown to promote anabolic pathways, including glycolysis (Bauer et al., 2004). mTORC1 coordinates cellular nutrient and energy states with anabolic metabolism to support cell growth and proliferation (Condon and Sabatini, 2019; Valvezan and Manning, 2019). The relationship between cytokine production and mTORC1-driven anabolic metabolism in pDCs aligned with findings that SLE patients who receive treatment with the mTORC1 inhibitor sirolimus show improvements in disease signs and symptoms (Eriksson et al., 2019; Lai et al., 2018). While IL-3-dependent production of cytokines by TLR-stimulated pDCs correlated with mTORC1 activity, we found that the effects of IL-3 alone on mTORC1 were limited. However, in the absence of IL-3 or GM-CSF, mTORC1 was not activated in response to TLR stimulation. We reasoned that this is consistent with the fact that the upstream activation of mTORC1 involves coordinated sensing of nutrients, in particular amino acids, for lysosomal translocation of mTORC1 with induction of its kinase activity (Condon and Sabatini, 2019; Sabatini, 2017). In this context, previous work in T cells pointed to a fundamental role for system LAA transporters in mTORC1 activation (Sinclair et al., 2019; Sinclair et al., 2013). Our data show that IL-3 or GM-CSF induce expression of *SLC7A5* and *SLC3A2* in pDCs, indicating that these cytokines initiate the nutrient-sensing pathway by permitting LNAA uptake and argue that this is the critical mTORC1-priming event that allows its activation in response to stimulation with TLR agonists. The ability of JAK2 inhibitors, which are downstream of IL-3 or GM-CSF receptors, to block *SLC7A5* and *SLC3A2* expression and therefore TLR-driven mTORC1 activation and IFN-α and TNF production strongly supports this contention.

We observed that *SLC7A5* and *SLC3A2* were expressed in circulating pDCs and able to transport kynurenine, even in HDs. This suggests that IL-3 and/or GM-CSF are available to pDCs in blood and that the cells circulate in a state where they are primed to respond to TLR stimulation. A critical event in pathological pDC activation may be the continued availability of IL-3 and/or GM-CSF to maintain pDC responsiveness as the cells leave the bloodstream and enter inflamed tissues. Tissue cells can make GM-CSF (Mascia et al., 2010), and tissue-infiltrating CD4 positive T cells would be expected to serve as a source of these cytokines once adaptive responses are established (Kunnath-Velayudhan et al., 2019; Leonard et al., 2016).

We found that activation via TLR7 and TLR9 diversified otherwise equally stimulated cells into subpopulations based on expression of system LAA transporters and mTORC1 activity, where only a population that acquired both of these features was able to produce cytokines. The emergence of a subset of type I IFN-producing cells enriched for TNF transcripts in TLR9-activated pDCs was also apparent in scRNA-seq analysis. This is reminiscent of a previous report that only a subset of *in vitro* TLR7-activated pDCs produce IFN-α and that an equivalent population can be found within pDCs from SLE patients (Alculumbre et al., 2018). We found that inhibitors that target JAK2 caused a decrease in IFN-α and TNF production linked to reductions in *SLC7A5* and *SLC3A2* expression and mTORC1 activity in TLR-activated pDCs, arguing that the subset of activated cells that may play a pathological role during disease could be inhibited in this fashion. In this context, JAK2-STAT5 signaling is engaged upon binding of IL-3 or GM-CSF to their receptors (Dougan et al., 2019), and JAK-STAT signaling, like type I IFN, is implicated in the development of autoimmunity (Schwartz et al., 2016). TOF, a pan-JAK inhibitor, has been reported to reduce IFN-α production by activated pDCs *in vitro* (Boor et al., 2017). More recently, BAR, a JAK1 and 2 inhibitor, has been successfully clinically trialed in SLE patients (Wallace et al., 2018). The mode of action of these inhibitors is believed to be largely due to their ability to inhibit JAK1 downstream of IFNA receptor and thereby to inhibit autocrine and paracrine effects of type I IFN. However, our data show that the effects of BAR or TOF can be recapitulated by the JAK2-preferential inhibitor AZD (Hedvat et al., 2009; Ioannidis et al., 2011). This raises the possibility that beneficial effects of BAR and TOF in SLE patients may reflect inhibitory effects on JAK2 rather than, or in addition to, effects on JAK1. In this context, we also showed that the expression of chemokines implicated in lupus was associated with *IFNA2* expression and susceptible to JAK2 inhibition. It is likely then that therapeutic effects of these drugs in SLE may be due to broader effects than the inhibition of type I IFN production.

One common consequence of TLR9 ligation found within the *in vitro* type I IFN- and TNF-producing pDCs and pDCs from pathological sites in SLE-induced lupus nephritis was hierarchical differential expression of 3 genes, *SLC7A11*, *ENPP2*, and *MYO1E*. We found that *SLC7A11* could regulate expression of *ENPP2* and *MYO1E* in activated pDCs. ENPP2 encodes autotaxin, an enzyme that catalyzes formation of extracellular

**Figure 6. Coordinated inhibition of JAK2 and $x_c^-$ synergize to block cytokine production**

(A–C, G, and J) Isolated pDCs were maintained ± IL-3 and indicated inhibitors o/n then stimulated ± CpG-A for 5 h and probed for: (A and J) IFN-α production or TNF production (A, IFN-α: n = 9–13 in 3–5 experiments, TNF: n = 4 in 1 experiment; (J) n = 6 in 2 experiments); (B) kynurenine uptake and pS6 expression (n = 5–9 in 2–4 experiments); (C) IFN-α production (n = 5–9 in 2–4 experiments); and (G) *ENPP2* or *MYO1E* mRNA expression (n = 4 in 2 experiments, CpG-A condition shared with Figure 5K).

(D–F) Isolated pDCs were maintained in regular or cystine-free media plus IL-3 o/n then stimulated ± CpG-A for 5 h and probed for: (D) IFN-α or TNF production; (E) kynurenine uptake and pS6 expression; and (F) pS6 expression (D–F, n = 6 in 2 experiments, untreated and CpG-A conditions shared with Figures 3F, 3G, S3G, and S3H).

(H, I, K, and L) Isolated pDCs were maintained in HPLM ± IL-3 with indicated inhibitors o/n then stimulated ± CpG-A for 5 h and probed for: (H and K) kynurenine uptake and pS6 expression; (I and L) IFN-α or TNF production (H and I, n = 7 in 2 experiments, 1 experiment shown; K and L, n = 6–8 in 3 experiments).

Representative plots from individual donors (n, see above) are shown (B). Bar graphs are shown as (A and J) geometric mean ± geometric SD, (C, D, F, G, I, and L) mean ± SD, and (E, H, and K) mean. Dots represent individual donors (n).

Please also see Figure S6.

lysophosphatidic acid (LPA), which is implicated in a variety of autoinflammatory and autoimmune conditions (Castelino et al., 2016; Ninou et al., 2018). Presently, we do not know whether activated pDCs produce LPA due to increased ENPP2 activity nor whether they are directly responsive to LPA, but nevertheless, our data show that the ENPP2 inhibitor ZIR is able to block production of IFN-$\alpha$ and TNF by activated pDCs. A detailed understanding of the function of ENPP2 in pDCs awaits further study. We currently have no data on the function of *MYO1E* in pDCs but speculate that it may be involved in membrane vesicular transport (Navinés-Ferrer and Martin, 2020).

As in T and B cells, where SLC7A11 is induced upon activation (Siska et al., 2016), we found that *SLC7A11* was expressed only by TLR-stimulated pDCs. In contrast to *SLC7A5*, *SLC7A11* was not expressed by circulating pDCs. These data indicate that SLC7A11 is a marker of inflammatory cytokine-producing tissue pDCs. SLC7A11 expression is believed to be regulated by Nrf2 (Lewerenz et al., 2013) or through mTORC1 (Park et al., 2017). We observed that expression of *SLC7A11* was inhibited by RAP and TOR, indicating that it was under the control of mTORC1. *ENPP2* and *MYO1E* expression was also regulated by mTORC1. IL-3 depletion and JAK2 inhibitors also prevented expression of *SLC7A11*, *ENPP2*, and *MYO1E* in response to TLR agonists, and we argue that this is due to their ability to effectively inhibit the upstream steps that are critical for mTORC1 activation. Accordingly, only cells that co-expressed *SLC7A11* and *SLC7A5* had the capacity to produce IFN-$\alpha$ after TLR9 stimulation. In this context, loss of SLC7A11 function has been demonstrated to have beneficial effects in experimental inflammatory conditions (Albertini et al., 2018; Merckx et al., 2017). In addition, based on our data and previous findings (Daher et al., 2019), we speculate that the dominant function of SLC7A11 may reflect its feedback role in sustaining mTORC1 activity. Considering the importance for pDC activation of sequential IL-3- or GM-CSF-induced expression of system LAA transporters and TLR-regulated tissue-specific expression of SLC7A11, we speculate that combination therapy using JAK2 and $x_c^-$ inhibitors may be beneficial for targeted inhibition of pDCs at sites of inflammation to treat diseases such as SLE.

## LIMITATION OF THE STUDY

We did not broadly assess transcriptional profiles of pDCs from a range of autoimmune conditions and how they relate to *in vitro*-activated pDCs. Therefore, we can only speculate that SLC7A11 is expressed in activated tissue-residing pDCs in diseases other than lupus nephritis. We neither defined the mechanism(s) through which SLC7A11 or ENPP2 play roles in pDC activation nor explored the functional significance of MYO1E expression. Our conclusions regarding the therapeutic potential of combinatorial inhibition of JAK2 and SLC7A11 are based on *in vitro* experiments.

## STAR★METHODS

Detailed methods are provided in the online version of this paper and include the following:



## SUPPLEMENTAL INFORMATION

Supplemental information can be found online at https://doi.org/10.1016/j.immuni.2021.10.009.

## ACKNOWLEDGMENTS

The authors thank Gustavo Carrizo, Mauro Corrado, Johan Friden, Beth Kelly, and Nisha Rana for helpful discussions, Jan Zamek at Cologne University for technical assistance with immunohistochemistry, and Theresa Schleyer at the ImmRheum Biobank for PBMCs from SLE patients. We also thank the core facilities (Deep Sequencing, Metabolomics, and Flow Cytometry) at the Max Planck of Immunobiology and Epigenetics for technical support. This work was supported by NIH AI 110481 (E.J.P.); German Research Foundation (DFG) SFB1160; DFG under Germany's Excellence Strategy (CIBSS EXC-2189 project ID 390939984); the Alexander von Humboldt Fellowship Foundation (A.M.K. and M.V.); Swiss National Science Foundation (M.M.); Japan Society for the Promotion of Science (M.M.); DK Cell Communication in Health and Disease W 1205-B09 (S.Z.); DFG, TRR130, project 12 to R.E.V.; and the Max Planck Society.

## AUTHOR CONTRIBUTIONS

Conceptualization, K.M.G., E.J.P.; procedures K.M.G., A.M.K., M.A.S., J.E.-H., M.M., A.H., F.H., S.Z., P.Z.; bioinformatics, D.E.S.; idata interpretation, K.M.G., D.E.S., J.E.-H., P.Z., E.J.P.; providing advice, materials, R.E.V., D.M.K., M.F., E.L.P.; project insights, K.M.G., D.E.S., A.M.K., M.F., E.L.P., E.J.P.; writing, K.M.G., E.J.P.; funding acquisition, E.J.P., E.L.P.; supervision: E.J.P.

## DECLARATION OF INTERESTS

K.M.G., D.E.S., and E.J.P. have filed a provisional patent application: Combined inhibition of amino acid transporters for inhibiting human pDC activity during autoimmunity. E.J.P. and E.L.P. are founders of Rheos Medicines. E.L.P. is a member of the SAB for ImmunoMet Therapeutics.

## INCLUSION AND DIVERSITY

We worked to ensure sex balance in the selection of non-human subjects. One or more of the authors of this paper self-identifies as living with a disability. One or more of the authors of this paper received support from a program designed to increase minority representation in science.

Received: August 29, 2020
Revised: July 1, 2021
Accepted: October 12, 2021
Published: October 29, 2021

## REFERENCES

Albertini, G., Deneyer, L., Ottestad-Hansen, S., Zhou, Y., Ates, G., Walrave, L., Demuyser, T., Bentea, E., Sato, H., De Bundel, D., et al. (2018). Genetic deletion of xCT attenuates peripheral and central inflammation and mitigates LPS-induced sickness and depressive-like behavior in mice. Glia *66*, 1845–1861.

Alculumbre, S.G., Saint-André, V., Di Domizio, J., Vargas, P., Sirven, P., Bost, P., Maurin, M., Maiuri, P., Wery, M., Roman, M.S., et al. (2018). Diversification of human plasmacytoid predendritic cells in response to a single stimulus. Nat. Immunol. *19*, 63–75.

Arazi, A., Rao, D.A., Berthier, C.C., Davidson, A., Liu, Y., Hoover, P.J., Chicoine, A., Eisenhaure, T.M., Jonsson, A.H., Li, S., et al.; Accelerating Medicines Partnership in SLE network (2019). The immune cell landscape in kidneys of patients with lupus nephritis. Nat. Immunol. *20*, 902–914.

Baccala, R., Gonzalez-Quintial, R., Blasius, A.L., Rimann, I., Ozato, K., Kono, D.H., Beutler, B., and Theofilopoulos, A.N. (2013). Essential requirement for IRF8 and SLC15A4 implicates plasmacytoid dendritic cells in the pathogenesis of lupus. Proc. Natl. Acad. Sci. USA *110*, 2940–2945.

Bajwa, G., DeBerardinis, R.J., Shao, B., Hall, B., Farrar, J.D., and Gill, M.A. (2016). Cutting Edge: Critical Role of Glycolysis in Human Plasmacytoid Dendritic Cell Antiviral Responses. J. Immunol. *196*, 2004–2009.

Basit, F., Mathan, T., Sancho, D., and de Vries, I.J.M. (2018). Human Dendritic Cell Subsets Undergo Distinct Metabolic Reprogramming for Immune Response. Front. Immunol. *9*, 2489.

Bassi, M.T., Gasol, E., Manzoni, M., Pineda, M., Riboni, M., Martín, R., Zorzano, A., Borsani, G., and Palacín, M. (2001). Identification and characterisation of human xCT that co-expresses, with 4F2 heavy chain, the amino acid transport activity system xc-. Pflugers Arch. *442*, 286–296.

Bauer, D.E., Harris, M.H., Plas, D.R., Lum, J.J., Hammerman, P.S., Rathmell, J.C., Riley, J.L., and Thompson, C.B. (2004). Cytokine stimulation of aerobic glycolysis in hematopoietic cells exceeds proliferative demand. FASEB J. *18*, 1303–1305.

Bhardwaj, V., Heyne, S., Sikora, K., Rabbani, L., Rauer, M., Kilpert, F., Richter, A.S., Ryan, D.P., and Manke, T. (2019). snakePipes: facilitating flexible, scalable and integrative epigenomic analysis. Bioinformatics *35*, 4757–4759.

Blanco, P., Palucka, A.K., Gill, M., Pascual, V., and Banchereau, J. (2001). Induction of dendritic cell differentiation by IFN-alpha in systemic lupus erythematosus. Science *294*, 1540–1543.

Boor, P.P.C., de Ruiter, P.E., Asmawidjaja, P.S., Lubberts, E., van der Laan, L.J.W., and Kwekkeboom, J. (2017). JAK-inhibitor tofacitinib suppresses interferon alfa production by plasmacytoid dendritic cells and inhibits arthrogenic and antiviral effects of interferon alfa. Transl. Res. *188*, 67–79.

Cantor, J.R., Abu-Remaileh, M., Kanarek, N., Freinkman, E., Gao, X., Louissaint, A., Jr., Lewis, C.A., and Sabatini, D.M. (2017). Physiologic Medium Rewires Cellular Metabolism and Reveals Uric Acid as an Endogenous Inhibitor of UMP Synthase. Cell *169*, 258–272.e17.

Cao, W., Manicassamy, S., Tang, H., Kasturi, S.P., Pirani, A., Murthy, N., and Pulendran, B. (2008). Toll-like receptor-mediated induction of type I interferon in plasmacytoid dendritic cells requires the rapamycin-sensitive PI(3)K-mTOR-p70S6K pathway. Nat. Immunol. *9*, 1157–1164.

Castelino, F.V., Bain, G., Pace, V.A., Black, K.E., George, L., Probst, C.K., Goulet, L., Lafyatis, R., and Tager, A.M. (2016). An Autotaxin/Lysophosphatidic Acid/Interleukin-6 Amplification Loop Drives Scleroderma Fibrosis. Arthritis Rheumatol. *68*, 2964–2974.

Cederblad, B., Blomberg, S., Vallin, H., Perers, A., Alm, G.V., and Rönnblom, L. (1998). Patients with systemic lupus erythematosus have reduced numbers of circulating natural interferon-alpha- producing cells. J. Autoimmun. *11*, 465–470.

Cella, M., Jarrossay, D., Facchetti, F., Alebardi, O., Nakajima, H., Lanzavecchia, A., and Colonna, M. (1999). Plasmacytoid monocytes migrate to inflamed lymph nodes and produce large amounts of type I interferon. Nat. Med. *5*, 919–923.

Chauvin, C., Koka, V., Nouschi, A., Mieulet, V., Hoareau-Aveilla, C., Dreazen, A., Cagnard, N., Carpentier, W., Kiss, T., Meyuhas, O., and Pende, M. (2014). Ribosomal protein S6 kinase activity controls the ribosome biogenesis transcriptional program. Oncogene *33*, 474–483.

Chidley, C., Haruki, H., Pedersen, M.G., Muller, E., and Johnsson, K. (2011). A yeast-based screen reveals that sulfasalazine inhibits tetrahydrobiopterin biosynthesis. Nat. Chem. Biol. *7*, 375–383.

Choi, J., and Fenando, A. (2020). Sulfasalazine. StatPearls (StatPearls Publishing).

Colonna, M., Trinchieri, G., and Liu, Y.J. (2004). Plasmacytoid dendritic cells in immunity. Nat. Immunol. *5*, 1219–1226.

Conaghan, P.G., Østergaard, M., Bowes, M.A., Wu, C., Fuerst, T., van der Heijde, D., Irazoque-Palazuelos, F., Soto-Raices, O., Hrycaj, P., Xie, Z., et al. (2016). Comparing the effects of tofacitinib, methotrexate and the combination, on bone marrow oedema, synovitis and bone erosion in methotrexate-naive, early active rheumatoid arthritis: results of an exploratory randomised MRI study incorporating semiquantitative and quantitative techniques. Ann. Rheum. Dis. *75*, 1024–1033.

Condon, K.J., and Sabatini, D.M. (2019). Nutrient regulation of mTORC1 at a glance. J. Cell Sci. *132*, jcs222570.

Conway, J.R., Lex, A., and Gehlenborg, N. (2017). UpSetR: an R package for the visualization of intersecting sets and their properties. Bioinformatics *33*, 2938–2940.

Daher, B., Parks, S.K., Durivault, J., Cormerais, Y., Baidarjad, H., Tambutte, E., Pouysségur, J., and Vučetić, M. (2019). Genetic Ablation of the Cystine Transporter xCT in PDAC Cells Inhibits mTORC1, Growth, Survival, and Tumor Formation via Nutrient and Oxidative Stresses. Cancer Res. *79*, 3877–3890.

Desroy, N., Housseman, C., Bock, X., Joncour, A., Bienvenu, N., Cherel, L., Labeguere, V., Rondet, E., Peixoto, C., Grassot, J.M., et al. (2017). Discovery of 2-[[2-Ethyl-6-[4-[2-(3-hydroxyazetidin-1-yl)-2-oxoethyl]piperazin-1-yl]-8-methylimidazo[1,2-a]pyridin-3-yl]methylamino]-4-(4-fluorophenyl) thiazole-5-carbonitrile (GLPG1690), a First-in-Class Autotaxin Inhibitor Undergoing Clinical Evaluation for the Treatment of Idiopathic Pulmonary Fibrosis. J. Med. Chem. *60*, 3580–3590.

Dixon, S.J., Patel, D.N., Welsch, M., Skouta, R., Lee, E.D., Hayano, M., Thomas, A.G., Gleason, C.E., Tatonetti, N.P., Slusher, B.S., and Stockwell, B.R. (2014). Pharmacological inhibition of cystine-glutamate exchange induces endoplasmic reticulum stress and ferroptosis. eLife *3*, e02523.

Dougan, M., Dranoff, G., and Dougan, S.K. (2019). GM-CSF, IL-3, and IL-5 Family of Cytokines: Regulators of Inflammation. Immunity *50*, 796–811.

Dzionek, A., Sohma, Y., Nagafune, J., Cella, M., Colonna, M., Facchetti, F., Günther, G., Johnston, I., Lanzavecchia, A., Nagasaka, T., et al. (2001). BDCA-2, a novel plasmacytoid dendritic cell-specific type II C-type lectin, mediates antigen capture and is a potent inhibitor of interferon alpha/beta induction. J. Exp. Med. *194*, 1823–1834.

Endo, A., Hasumi, K., Sakai, K., and Kanbe, T. (1985). Specific inhibition of glyceraldehyde-3-phosphate dehydrogenase by koningic acid (heptelidic acid). J. Antibiot. (Tokyo) *38*, 920–925.

Eriksson, P., Wallin, P., and Sjöwall, C. (2019). Clinical Experience of Sirolimus Regarding Efficacy and Safety in Systemic Lupus Erythematosus. Front. Pharmacol. *10*, 82.

Fishman, P., Kamashta, M., Ehrenfeld, M., Vianna, J., Hughes, G.R., Sredni, D., Zigelman, R., Sabo, G., and Shoenfeld, Y. (1993). Interleukin-3 immunoassay in systemic lupus erythematosus patients: preliminary data. Int. Arch. Allergy Immunol. *100*, 215–218.

Ghirelli, C., Zollinger, R., and Soumelis, V. (2010). Systematic cytokine receptor profiling reveals GM-CSF as a novel TLR-independent activator of human plasmacytoid predendritic cells. Blood *115*, 5037–5040.

Gilliet, M., Cao, W., and Liu, Y.J. (2008). Plasmacytoid dendritic cells: sensing nucleic acids in viral infection and autoimmune diseases. Nat. Rev. Immunol. *8*, 594–606.

Gottschalk, T.A., Tsantikos, E., and Hibbs, M.L. (2015). Pathogenic Inflammation and Its Therapeutic Targeting in Systemic Lupus Erythematosus. Front. Immunol. *6*, 550.

Gout, P.W., Buckley, A.R., Simms, C.R., and Bruchovsky, N. (2001). Sulfasalazine, a potent suppressor of lymphoma growth by inhibition of the x(c)- cystine transporter: a new action for an old drug. Leukemia *15*, 1633–1640.

Grouard, G., Rissoan, M.-C., Filgueira, L., Durand, I., Banchereau, J., and Liu, Y.-J. (1997). The enigmatic plasmacytoid T cells develop into dendritic cells with interleukin (IL)-3 and CD40-ligand. J. Exp. Med. *185*, 1101–1111.

Hedvat, M., Huszar, D., Herrmann, A., Gozgit, J.M., Schroeder, A., Sheehy, A., Buettner, R., Proia, D., Kowolik, C.M., Xin, H., et al. (2009). The JAK2 inhibitor AZD1480 potently blocks Stat3 signaling and oncogenesis in solid tumors. Cancer Cell *16*, 487–497.

Ioannidis, S., Lamb, M.L., Wang, T., Almeida, L., Block, M.H., Davies, A.M., Peng, B., Su, M., Zhang, H.J., Hoffmann, E., et al. (2011). Discovery of 5-chloro-N2-[(1S)-1-(5-fluoropyrimidin-2-yl)ethyl]-N4-(5-methyl-1H-pyrazol-3-yl)pyrimidine-2,4-diamine (AZD1480) as a novel inhibitor of the Jak/Stat pathway. J. Med. Chem. *54*, 262–276.

Jegalian, A.G., Facchetti, F., and Jaffe, E.S. (2009). Plasmacytoid dendritic cells: physiologic roles and pathologic states. Adv. Anat. Pathol. *16*, 392–404.

Karrich, J.J., Jachimowski, L.C., Uittenbogaart, C.H., and Blom, B. (2014). The plasmacytoid dendritic cell as the Swiss army knife of the immune system: molecular regulation of its multifaceted functions. J. Immunol. *193*, 5772–5778.

Kunnath-Velayudhan, S., Goldberg, M.F., Saini, N.K., Ng, T.W., Arora, P., Johndrow, C.T., Saavedra-Avila, N.A., Johnson, A.J., Xu, J., Kim, J., et al. (2019). Generation of IL-3-Secreting CD4$^{+}$ T Cells by Microbial Challenge at Skin and Mucosal Barriers. Immunohorizons *3*, 161–171.

Lai, Z.-W., Kelly, R., Winans, T., Marchena, I., Shadakshari, A., Yu, J., Dawood, M., Garcia, R., Tily, H., Francis, L., et al. (2018). Sirolimus in patients with clinically active systemic lupus erythematosus resistant to, or intolerant of, conventional medications: a single-arm, open-label, phase 1/2 trial. Lancet *391*, 1186–1196.

Lam, G.K., and Petri, M. (2005). Assessment of systemic lupus erythematosus. Clin. Exp. Rheumatol. *23* (5, Suppl 39), S120–S132.

Lande, R., Gregorio, J., Facchinetti, V., Chatterjee, B., Wang, Y.H., Homey, B., Cao, W., Wang, Y.H., Su, B., Nestle, F.O., et al. (2007). Plasmacytoid dendritic cells sense self-DNA coupled with antimicrobial peptide. Nature *449*, 564–569.

Lardy, H.A., Johnson, D., and McMURRAY, W.C. (1958). Antibiotics as tools for metabolic studies. I. A survey of toxic antibiotics in respiratory, phosphorylative and glycolytic systems. Arch. Biochem. Biophys. *78*, 587–597.

Leonard, D., Eloranta, M.L., Hagberg, N., Berggren, O., Tandre, K., Alm, G., and Rönnblom, L. (2016). Activated T cells enhance interferon-$\alpha$ production by plasmacytoid dendritic cells stimulated with RNA-containing immune complexes. Ann. Rheum. Dis. *75*, 1728–1734.

Lewerenz, J., Hewett, S.J., Huang, Y., Lambros, M., Gout, P.W., Kalivas, P.W., Massie, A., Smolders, I., Methner, A., Pergande, M., et al. (2013). The cystine/glutamate antiporter system x(c)(-) in health and disease: from molecular mechanisms to novel therapeutic opportunities. Antioxid. Redox Signal. *18*, 522–555.

Liao, X., Pirapakaran, T., and Luo, X.M. (2016). Chemokines and Chemokine Receptors in the Development of Lupus Nephritis. Mediators Inflamm. *2016*, 6012715.

Liu, Y.J. (2005). IPC: professional type 1 interferon-producing cells and plasmacytoid dendritic cell precursors. Annu. Rev. Immunol. *23*, 275–306.

Loewith, R., Jacinto, E., Wullschleger, S., Lorberg, A., Crespo, J.L., Bonenfant, D., Oppliger, W., Jenoe, P., and Hall, M.N. (2002). Two TOR complexes, only one of which is rapamycin sensitive, have distinct roles in cell growth control. Mol. Cell *10*, 457–468.

Maidhof, W., and Hilas, O. (2012). Lupus: an overview of the disease and management options. P&T *37*, 240–249.

Markham, A. (2017). Baricitinib: First Global Approval. Drugs *77*, 697–704.

Mascia, F., Cataisson, C., Lee, T.C., Threadgill, D., Mariani, V., Amerio, P., Chandrasekhara, C., Souto Adeva, G., Girolomoni, G., Yuspa, S.H., and Pastore, S. (2010). EGFR regulates the expression of keratinocyte-derived granulocyte/macrophage colony-stimulating factor in vitro and in vivo. J. Invest. Dermatol. *130*, 682–693.

McInnes, L., Healy, J., Saul, N., and Großberger, L. (2018). UMAP: Uniform Manifold Approximation and Projection. J. Open Source Softw. *3*, 861.

Merckx, E., Albertini, G., Paterka, M., Jensen, C., Albrecht, P., Dietrich, M., Van Liefferinge, J., Bentea, E., Verbruggen, L., Demuyser, T., et al. (2017). Absence of system $x_c^-$ on immune cells invading the central nervous system alleviates experimental autoimmune encephalitis. J. Neuroinflammation *14*, 9.

Morand, E.F., Furie, R., Tanaka, Y., Bruce, I.N., Askanase, A.D., Richez, C., Bae, S.C., Brohawn, P.Z., Pineda, L., Berglind, A., and Tummala, R.; TULIP-2 Trial Investigators (2020). Trial of Anifrolumab in Active Systemic Lupus Erythematosus. N. Engl. J. Med. *382*, 211–221.

Mui, A.L., Wakao, H., O'Farrell, A.M., Harada, N., and Miyajima, A. (1995). Interleukin-3, granulocyte-macrophage colony stimulating factor and interleukin-5 transduce signals through two STAT5 homologs. EMBO J. *14*, 1166–1175.

Murphy, G., and Isenberg, D.A. (2019). New therapies for systemic lupus erythematosus - past imperfect, future tense. Nat. Rev. Rheumatol. *15*, 403–412.

Navinés-Ferrer, A., and Martín, M. (2020). Long-Tailed Unconventional Class I Myosins in Health and Disease. Int. J. Mol. Sci. *21*, 2555.

Ninou, I., Magkrioti, C., and Aidinis, V. (2018). Autotaxin in Pathophysiology and Pulmonary Fibrosis. Front. Med. (Lausanne) *5*, 180.

Oda, K., Hosoda, N., Endo, H., Saito, K., Tsujihara, K., Yamamura, M., Sakata, T., Anzai, N., Wempe, M.F., Kanai, Y., and Endou, H. (2010). L-type amino acid transporter 1 inhibitors inhibit tumor cell growth. Cancer Sci. *101*, 173–179.

Oh, B.M., Lee, S.J., Park, G.L., Hwang, Y.S., Lim, J., Park, E.S., Lee, K.H., Kim, B.Y., Kwon, Y.T., Cho, H.J., and Lee, H.G. (2019). Erastin Inhibits Septic Shock and Inflammatory Gene Expression via Suppression of the NF-$\kappa$B Pathway. J. Clin. Med. *8*, 2210.

Olweus, J., BitMansour, A., Warnke, R., Thompson, P.A., Carballido, J., Picker, L.J., and Lund-Johansen, F. (1997). Dendritic cell ontogeny: a human dendritic cell lineage of myeloid origin. Proc. Natl. Acad. Sci. USA *94*, 12551–12556.

Oon, S., Huynh, H., Tai, T.Y., Ng, M., Monaghan, K., Biondo, M., Vairo, G., Maraskovsky, E., Nash, A.D., Wicks, I.P., and Wilson, N.J. (2016). A cytotoxic anti-IL-3R$\alpha$ antibody targets key cells and cytokines implicated in systemic lupus erythematosus. JCI Insight *1*, e86131.

Oon, S., Monaghan, K., Ng, M., Hoi, A., Morand, E., Vairo, G., Maraskovsky, E., Nash, A.D., Wicks, I.P., and Wilson, N.J. (2019). A potential association between IL-3 and type I and III interferons in systemic lupus erythematosus. Clin. Transl. Immunology *8*, e01097.

Park, Y., Reyna-Neyra, A., Philippe, L., and Thoreen, C.C. (2017). mTORC1 Balances Cellular Amino Acid Supply with Demand for Protein Synthesis through Post-transcriptional Control of ATF4. Cell Rep. *19*, 1083–1090.

Piqueras, B., Connolly, J., Freitas, H., Palucka, A.K., and Banchereau, J. (2006). Upon viral exposure, myeloid and plasmacytoid dendritic cells produce 3 waves of distinct chemokines to recruit immune effectors. Blood *107*, 2613–2618.

Reddy, E.P., Korapati, A., Chaturvedi, P., and Rane, S. (2000). IL-3 signaling and the role of Src kinases, JAKs and STATs: a covert liaison unveiled. Oncogene *19*, 2532–2547.

Reizis, B. (2019). Plasmacytoid Dendritic Cells: Development, Regulation, and Function. Immunity *50*, 37–50.

Sabatini, D.M. (2017). Twenty-five years of mTOR: Uncovering the link from nutrients to growth. Proc. Natl. Acad. Sci. USA *114*, 11818–11825.

Saxton, R.A., and Sabatini, D.M. (2017). mTOR Signaling in Growth, Metabolism, and Disease. Cell *168*, 960–976.

Schmidl, C., Hansmann, L., Lassmann, T., Balwierz, P.J., Kawaji, H., Itoh, M., Kawai, J., Nagao-Sato, S., Suzuki, H., Andreesen, R., et al.; FANTOM consortium (2014). The enhancer and promoter landscape of human regulatory and conventional T-cell subpopulations. Blood *123*, e68–e78.

Schwartz, D.M., Bonelli, M., Gadina, M., and O'Shea, J.J. (2016). Type I/II cytokines, JAKs, and new strategies for treating autoimmune diseases. Nat. Rev. Rheumatol. *12*, 25–36.

Siegal, F.P., Kadowaki, N., Shodell, M., Fitzgerald-Bocarsly, P.A., Shah, K., Ho, S., Antonenko, S., and Liu, Y.J. (1999). The nature of the principal type 1 interferon-producing cells in human blood. Science *284*, 1835–1837.

Sinclair, L.V., Howden, A.J., Brenes, A., Spinelli, L., Hukelmann, J.L., Macintyre, A.N., Liu, X., Thomson, S., Taylor, P.M., Rathmell, J.C., et al. (2019). Antigen receptor control of methionine metabolism in T cells. eLife *8*, e44210.

Sinclair, L.V., Neyens, D., Ramsay, G., Taylor, P.M., and Cantrell, D.A. (2018). Single cell analysis of kynurenine and System L amino acid transport in T cells. Nat. Commun. *9*, 1981.

Sinclair, L.V., Rolf, J., Emslie, E., Shi, Y.B., Taylor, P.M., and Cantrell, D.A. (2013). Control of amino-acid transport by antigen receptors coordinates the metabolic reprogramming essential for T cell differentiation. Nat. Immunol. *14*, 500–508.

Sisirak, V., Ganguly, D., Lewis, K.L., Couillault, C., Tanaka, L., Bolland, S., D'Agati, V., Elkon, K.B., and Reizis, B. (2014). Genetic evidence for the role of plasmacytoid dendritic cells in systemic lupus erythematosus. J. Exp. Med. *211*, 1969–1976.

Siska, P.J., Kim, B., Ji, X., Hoeksema, M.D., Massion, P.P., Beckermann, K.E., Wu, J., Chi, J.T., Hong, J., and Rathmell, J.C. (2016). Fluorescence-based measurement of cystine uptake through xCT shows requirement for ROS detoxification in activated lymphocytes. J. Immunol. Methods *438*, 51–58.

Stuart, T., Butler, A., Hoffman, P., Hafemeister, C., Papalexi, E., Mauck, W.M., 3rd, Hao, Y., Stoeckius, M., Smibert, P., and Satija, R. (2019). Comprehensive Integration of Single-Cell Data. Cell *177*, 1888–1902.e1821.

Swiecki, M., and Colonna, M. (2015). The multifaceted biology of plasmacytoid dendritic cells. Nat. Rev. Immunol. *15*, 471–485.

Thoreen, C.C., Chantranupong, L., Keys, H.R., Wang, T., Gray, N.S., and Sabatini, D.M. (2012). A unifying model for mTORC1-mediated regulation of mRNA translation. Nature *485*, 109–113.

Thoreen, C.C., Kang, S.A., Chang, J.W., Liu, Q., Zhang, J., Gao, Y., Reichling, L.J., Sim, T., Sabatini, D.M., and Gray, N.S. (2009). An ATP-competitive mammalian target of rapamycin inhibitor reveals rapamycin-resistant functions of mTORC1. J. Biol. Chem. *284*, 8023–8032.

Valvezan, A.J., and Manning, B.D. (2019). Molecular logic of mTORC1 signalling as a metabolic rheostat. Nat. Metab. *1*, 321–333.

Vander Heiden, M.G., Plas, D.R., Rathmell, J.C., Fox, C.J., Harris, M.H., and Thompson, C.B. (2001). Growth factors can influence cell growth and survival through effects on glucose metabolism. Mol. Cell. Biol. *21*, 5899–5912.

Verrey, F., Closs, E.I., Wagner, C.A., Palacin, M., Endou, H., and Kanai, Y. (2004). CATs and HATs: the SLC7 family of amino acid transporters. Pflugers Arch. *447*, 532–542.

Wallace, D.J., Furie, R.A., Tanaka, Y., Kalunian, K.C., Mosca, M., Petri, M.A., Dörner, T., Cardiel, M.H., Bruce, I.N., Gomez, E., et al. (2018). Baricitinib for systemic lupus erythematosus: a double-blind, randomised, placebo-controlled, phase 2 trial. Lancet *392*, 222–231.

Willeke, P., Schlüter, B., Schotte, H., Erren, M., Mickholz, E., Domschke, W., and Gaubitz, M. (2004). Increased frequency of GM-CSF secreting PBMC in patients with active systemic lupus erythematosus can be reduced by immunoadsorption. Lupus *13*, 257–262.

Wills, J., Edwards-Hicks, J., and Finch, A.J. (2017). AssayR: A Simple Mass Spectrometry Software Tool for Targeted Metabolic and Stable Isotope Tracer Analyses. Anal. Chem. *89*, 9616–9619.

Wu, D., Sanin, D.E., Everts, B., Chen, Q., Qiu, J., Buck, M.D., Patterson, A., Smith, A.M., Chang, C.H., Liu, Z., et al. (2016). Type 1 Interferons Induce Changes in Core Metabolism that Are Critical for Immune Function. Immunity *44*, 1325–1336.

Yagoda, N., von Rechenberg, M., Zaganjor, E., Bauer, A.J., Yang, W.S., Fridman, D.J., Wolpaw, A.J., Smukste, I., Peltier, J.M., Boniface, J.J., et al. (2007). RAS-RAF-MEK-dependent oxidative cell death involving voltage-dependent anion channels. Nature *447*, 864–868.

Zhang, Y., Liu, T., Meyer, C.A., Eeckhoute, J., Johnson, D.S., Bernstein, B.E., Nusbaum, C., Myers, R.M., Brown, M., Li, W., and Liu, X.S. (2008). Model-based analysis of ChIP-Seq (MACS). Genome Biol. *9*, R137.

## STAR★METHODS

### KEY RESOURCES TABLE

| REAGENT or RESOURCE | SOURCE | IDENTIFIER |
|---|---|---|
| **Antibodies** | | |
| Mouse monoclonal anti-CD123 (clone AC145) | Miltenyi Biotec | Cat# 130-090-897, RRID:AB_244210 |
| Mouse monoclonal anti-HLA-DR (clone G46-6 (L243)) | BD Biosciences | Cat# 556642, RRID:AB_396508 |
| Mouse monoclonal anti-CD303 (BDCA-2) (clone 201A) | BioLegend | Cat# 354205, RRID:AB_11147168 |
| Mouse monoclonal anti-CD116 (clone hGMCSFR-M1) | BD Biosciences | Cat# 747410, RRID:AB_2872098 |
| Rat monoclonal anti-CD4 (clone A161A1) | BioLegend | Cat# 357405, RRID:AB_2562356 |
| Mouse monoclonal anti-IFN-alpha (clone LT27:295) | Miltenyi Biotec | Cat# 130-092-600, RRID:AB_871559 |
| Mouse monoclonal anti-TNF-alpha (clone MAb11) | BioLegend | Cat# 502913, RRID:AB_315265 |
| Rabbit polyclonal anti-phospho-S6 ribosomal protein (Ser235/236) (D57.2.2E) | Cell Signaling Technology | Cat# 2211, RRID:AB_331679 |
| Rabbit monoclonal phospho-Stat5 (Tyr694) (C71E5) | Cell Signaling Technology | Cat# 9314, RRID:AB_2302702 |
| Rabbit polyclonal Anti-xCT (SLC7A11) | Abcam | Cat# ab37185,RRID:AB_778944 |
| Mouse monoclonal anti-CD123 (NCL-L-CD123) (clone BR4MS) | Novocastra/Leica | Cat# NCL-L-CD123, RRID:AB_10555271 |
| Goat anti-IgG (H+L) Highly Cross-Adsorbed Secondary Antibody | Thermo Fisher Scientific | Cat# A32723, RRID:AB_2633275 |
| Goat anti-IgG (H+L) Highly Cross-Adsorbed Secondary Antibody | Thermo Fisher Scientific | Cat# A32731, RRID:AB_2633280 |
| FcR blocking reagent, human | Miltenyi Biotec | Cat# 130-059-901 |
| **Biological samples** | | |
| Healthy donor blood | Institute for Transfusion Medicine and Gene Therapy, Medical Center – University of Freiburg | |
| Skin samples from lupus patients | University of Cologne, biobank of the SFB829 (Z4 project) | Ethics committee# 12-163 and 19-1146 |
| PBMCs and sera from systemic lupus erythematosus patients | ImmRheum biobank in Freiburg | Ethics committee # 507/16 and 624/14 |
| PBMCs from rheumatoid patients | University Hospital Cologne | Ethics committee # 13-091 |
| **Chemicals, peptides, and recombinant proteins** | | |
| Rapamycin | Calbiochem | Cat# 553211, CAS 53123-88-9 |
| Torin 1 | Tocris | Cat# 4247, CAS 1222998-36-8 |
| Heptelidic acid | AdipoGen | Cat# AG-CN2-0118, CAS 57710-57-3 |
| Oligomycin A | Sigma | Cat# 75351, CAS 579-13-5 |
| AZD 1480 | Selleckchem | Cat# S2162, CAS 935666-88-9 |
| Baricitinib | Selleckchem | Cat # S2851, CAS 1187594-09-7 |
| CP 690550 (Tofacitinib) | Tocris | Cat# 4556, CAS 540737-29-9 |
| Erastin | R&D | Cat# 5449, CAS 571203-78-6 |
| Erastin | Sigma | Cat# E7781, CAS 571203-78-6 |
| Sulfasalazine | Tocris | Cat# 4935, CAS 599-79-1 |
| JPH203 | Selleckchem | Cat# S8667, CAS 1037592-40-7 |
| Ziritaxestat | MCE MedChemExprress | Cat# HY-101772, CAS 1628260-79-6 |
| CpG-A (ODN2216) | InvivoGen | Cat# tlrl-2216 |

(*Continued on next page*)

*Continued*

| REAGENT or RESOURCE | SOURCE | IDENTIFIER |
|---|---|---|
| CpG-B (ODN2006) | InvivoGen | Cat# tlrl-2006 |
| CpG-C (ODN2395) | InvivoGen | Cat# tlrl-2395 |
| R837 (imiquimod) | InvivoGen | Cat# tlrl-imq |
| R848 (resiquimod) | InvivoGen | Cat# tlrl-4848 |
| 2-Mercaptoethanol | GIBCO | Cat# 31350-010 |
| Bovine Serum Albumin | GIBCO | Cat# A2153, CAS 9048-46-8 |
| Cycloheximide | Sigma | Cat# 0181, CAS 66-81-9 |
| L-kynurenine | Sigma | Cat# K8625, CAS 2922-83-0 |
| BCH | Tocris | Cat# 5027, CAS 20448-79-7 |
| Poly-D-Lysine | GIBCO | Cat# A3890401 |
| D-(+)-Glucose solution | Sigma-Aldrich | Cat# G8644, CAS 50-99-7 |
| LIVE/DEAD Fixable Near-IR Dead Cell Stain Kit | Invitrogen | Cat# L34975 |
| LIVE/DEAD Fixable Aqua Dead Cell Stain Kit | Invitrogen | Cat# L34957 |
| BD GolgiPlug | BD Bioscience | Cat# 555029 |
| D-glucose-13C6, 99 atom% 13C, $^{3}$99% | Sigma | Cat#389374 |
| Methanol | Sigma | Cat# 34860, CAS 67-56-1 |
| Acetonitrile | Sigma | Cat# 34851, CAS 75-05-8 |
| Amonium Carbonate | Sigma | Cat# 207861, CAS 506-87-6 |
| Amonium hydroxide solution | Sigma | Cat# 221228, CAS 1336-21-6 |
| Hylol | Sigma | Cat# 534056, CAS 1330-20-7 |
| Ethanol | Sigma | Cat# 1.11727, CAS 64-17-5 |
| Tris base | Sigma | Cat# TRIS-RO, CAS 77-86-1 |
| UltraPure 0.5M EDTA, pH 8.0 | Invitrogen | Cat# 5575020, CAS 60-00-4 |
| Tweeen 20 | Sigma | Cat# P9416, Cas 9005-64-5 |
| DAPI | Invitrogen | Cat# D1306, CAS 1H-Indole-6-carboximidamide, 2-[4-(aminoiminomethyl) phenyl]-, dihydrochloride 28718-90-3 |
| Alt-R S.p. Cas9 Nuclease V3 | IDT | 1081058 |
| **Critical commercial assays** | | |
| Plasmacytoid dendritic cell isolation kit II, human | Miltenyi Biotec | Cat# 130-097-415 |
| BD Cytfix/Cytoperm Fixation/Permeabilization Kit | BD Bioscience | Cat# 554714 |
| Click-iT Plus OPP Alexa Fluor 647 Protein Synthesis Assay Kit | Invitrogen | Cat# C10458 |
| PrimeFlow RNA Assay Kit | Invitrogen | Cat# 88-18005 |
| LEGENDplex Human Anti-Virus Response Panel (13-Plex) | BioLegend | Cat# 7410390 |
| Chromium Single Cell 3′ Reagent Kit (v2 Chemistry) | 10X Genomics | Cat# v2 no longer in use |
| **Deposited data** | | |
| scRNA-sequencing data | Arazi et al., 2019 | ImmPort: SDY997 |
| scRNA-sequencing data | This paper | GEO: GSE157305 |
| ChIP sequencing | Schmidl et al., 2014 | GEO: GSE43119 |
| **Oligonucleotides** | | |
| PrimeFlow Probe Set: IFNA2, type 6 | Invitrogen | Assay ID# VA6-16322-PF |
| PrimeFlow Probe Set: IFNA2, type 10 | Invitrogen | Assay ID# VA10-10651-PF |
| PrimeFlow Probe Set: TNF, type 1 | Invitrogen | Assay ID# VA1-10481-PF |
| PrimeFlow Probe Set: SLC7A5, type 6 | Invitrogen | Assay ID# VA6-3169319-PF |
| PrimeFlow Probe Set: SLC3A2, type 4 | Invitrogen | Assay ID# VA4-3088288-PF |
| PrimeFlow Probe Set: SLC7A11, type 1 | Invitrogen | Assay ID# VA1-3007681-PF |
| PrimeFlow Probe Set: ENPP2, type 4 | Invitrogen | Assay ID# VA4-3083016-PF |

(*Continued on next page*)

*Continued*

| REAGENT or RESOURCE | SOURCE | IDENTIFIER |
|---|---|---|
| PrimeFlow Probe Set: MYO1E, type 6 | Invitrogen | Assay ID# VA6-3168363-PF |
| PrimeFlow Probe Set: CCL3, type 1 | Invitrogen | Assay ID# VA1-15428-PF |
| PrimeFlow Probe Set: CCL17, type 6 | Invitrogen | Assay ID# VA6-18108-PF |
| PrimeFlow Probe Set: CXCL8, type 1 | Invitrogen | Assay ID# VA1-13103-PF |
| PrimeFlow Probe Set: CXCL9, type 1 | Invitrogen | Assay ID# VA1-14808-PF |
| PrimeFlow Probe Set: CXCL10, type 1 | Invitrogen | Assay ID# VA1-18213-PF |
| SLC3A2 gRNA1 | IDT | Hs.Cas9.SLC3A2.1.AB |
| SLC3A2 gRNA2 | IDT | Hs.Cas9.SLC3A2.1.AE |
| SLC7A5 gRNA1 | IDT | Hs.Cas9.SLC7A5.1.AA |
| SLC7A5 gRNA2 | IDT | Hs.Cas9.SLC7A5.1.AC |
| SLC7A11 gRNA1 | IDT | Hs.Cas9.SLC7A11.1.AA |
| SLC7A11 gRNA2 | IDT | Hs.Cas9.SLC7A11.1.AE |
| Non-targeting control gRNA | IDT | Hs.Cas9.GCGAGGTATTCGCTCCGCG |
| **Software and algorithms** | | |
| FlowJo v.9.9.6 | Tristar | https://www.flowjo.com |
| Graphpad Prism 7 | Graphpad software | http://www.graphpad.com |
| AssayR | Wills et al., 2017 | https://www.ncbi.nlm.nih.gov/pmc/articles/PMC5628912/ |
| Wave software version 2.4 | Agilent | http://www.agilent.com/cs/ContentServer?c = Page&pagename = Sapphire/Page/HomePage |
| Cell Ranger 2.2 | 10X Genomics | https://support.10xgenomics.com/single-cell-gene-expression/software/pipelines/latest/using/tutorial_in |
| Seurat v3 | Stuart et al., 2019 | https://pubmed.ncbi.nlm.nih.gov/31178118/ |
| Uniform Manifold Approximation and Projection | McInnes et al., 2018 | https://arxiv.org/abs/1802.03426 |
| UpSet | Conway et al., 2017 | https://pubmed.ncbi.nlm.nih.gov/28645171/ |
| snakePipe | Bhardwaj et al., 2019 | https://snakepipes.readthedocs.io/en/latest/index.html |
| MACS2 | Zhang et al., 2008 | https://pubmed.ncbi.nlm.nih.gov/18798982/ |
| **Other** | | |
| RPMI 1640 medium | GIBCO | Cat# 21875034 |
| RPMI 1640 w/o L-glutamine and L-leucine medium | MP Biomedicals | Cat# 09162914 |
| RPMI w/o L-cystine, L-glutamine and L-methionine medium | MP Biomedicals | Cat# 09164645 |
| RPMI w/o methionine | GIBCO | Cat# A1451701 |
| HPLM medium | GIBCO | Cat# A4899101 |
| Cytiva HyClone, Fetal Bovine Serum | Fisher Scientific | Cat# 16291082 |
| Cytiva HyClone, Fetal Bovine Serum, dialyzed | Fisher Scientific | Cat# 12379822 |
| L-glutamine 200 mM | GIBCO | Cat# 25030149 |
| L-methionine | Sigma | Cat# M9625 |
| Penicilin/Streptomycin 10,000 U/ml | GIBCO | Cat# 15140-122 |
| Recombinant human IL-3 | Peprotech | Cat# 200-03 |
| Recombinant human GM-CSF | Peprotech | Cat# 300-03 |
| PBS w/o calcium chloride and magnesium | GIBCO | Cat# 10010-015 |
| HBSS w/o calcium chloride and magnesium and phenol red | GIBCO | Cat# 14175095 |
| RPMI 1640 medium, powder | GIBCO | Cat# 31800105 |
| Sodium Pyruvate, 100 mM | GIBCO | Cat# 11360070 |
| Agilent Seahorse XF Calibrant | Agilent | Cat#100840-000 |
| Glucose Bio | Roche | Cat# 0634373200 |

(*Continued on next page*)

*Continued*

| REAGENT or RESOURCE | SOURCE | IDENTIFIER |
|---|---|---|
| Lactate Bio | Roche | Cat# 0634375900 |
| Normal goat serum | abcam | Cat# ab7481 |

## RESOURCE AVAILABILITY

### Lead contact

Further information and requests for resources and reagents should be directed to and will be fulfilled by the lead contact, Edward J. Pearce (epearce7@jhmi.edu).

### Materials availability

This study did not generate new unique reagents.

### Data and code availability

Single cell RNA-seq data have been deposited at GEO and are publicly available as of the date of publication. Accession numbers are listed in the key resources table.

This paper analyzes existing, publicly available data. These accession numbers for the datasets are listed in the key resources table.

Microscopy data reported in this paper will be shared by the lead contact upon request.

This paper does not report original code.

## EXPERIMENTAL MODEL AND SUBJECT DETAILS

### Human cells

Buffy coats were kindly provided by the Institute for Transfusion Medicine and Gene Therapy, Medical Center – University of Freiburg (donor consent, anonymized). Skin samples of lupus patients were obtained through the biobank of the SFB829 (Z4 project) with informed consent from all the subjects and ethical approval obtained from the Ethics Committee at the University of Cologne (votes 12-163 and 19-1146). SLE PBMCs and sera were provided by ImmRheum biobank in Freiburg, a project that was approved by the local ethical committee (votes 507/16 and 624/14). All patients who provided blood to the biobank had provided written informed consent. RA PBMCs were provided by the University Hospital Cologne, a project that was approved by the local ethical committee (number 13-091). Researchers were blinded to the identity of the donors, and age or sex matching was not performed. Sample size is indicated in the figure legends.

## METHOD DETAILS

### Cell isolation and culture

PBMCs from buffy coats from healthy blood donors were isolated by density gradient centrifugation using SepMate tubes and Lymphoprep (both STEMCELL Technologies). pDCs were negatively selected from PBMCs using the plasmacytoid dendritic cell isolation kit II (Miltenyi Biotec). Isolated pDCs were maintained in RPMI (GIBCO) supplemented with 10% FBS (HyClone), 2 mM L-glutamine (GIBCO), 10,000 U/ml Penicillin/Streptomycin (GIBCO), 55 μM β-Mercaptoethanol (Sigma) and, where indicated, 50 ng/ml recombinant human IL-3 (Peprotech) or 50 ng/ml recombinant human GM-CSF (Peprotech). Where indicated, cells were cultured in RPMI without L-leucine and L-glutamine (MP Biomedicals) supplemented 2 mM L-glutamine (GIBCO) or RPMI without methionine (GIBCO) or RPMI without L-cystine, L-glutamine and L-methionine (MP Biomedicals) supplemented with 2 mM L-glutamine (GIBCO) and 0.1 mM L-methionine (Sigma) or HPLM (GIBCO).

Amino acid free and HPLM media were supplemented with 10% dialyzed FBS (HyClone), 10,000 U/ml Penicillin/Streptomycin (GIBCO), 55 μM β-Mercaptoethanol (Sigma) and 50 ng/ml recombinant human IL-3 (Peprotech). Cells were stimulated with 5 μM CpG-A (ODN2216) or 5 μM CpG-B (ODN2006) or 5 μM CpG-C (ODN2395) or 0.5 μg/ml R848 (resiquimod) or 5 μg/ml R837 (imiquimod) (all from InvivoGen) for times indicated. To detect intracellular cytokines, cells were treated with GolgiPlug (BD Bioscience) for the last 4 h of the culture. For overnight (o/n) incubations, cells were plated at 0.5 - 1x$10^6$/ml. Where indicated, cells were treated with the following inhibitors: 20 nM rapamycin (Calbiochem), 250 nM torin1 (Tocris), 10 μM heptelidic acid (Adipogen), 1 μM oligomycin (Sigma), 1 μM AZD1480 (Selleckchem), 25 nM - 1 μM baricitinib (LY3009104, Selleckchem), 200 ng/ml tofacitinib (CP690550, Tocris), 5 or 10 μM erastin (R&D Systems or Sigma, respectively), 100 or 200 μM sulfasalazine (Tocris), 5 or 10 μM JPH203 (KYT-0353, Selleckchem), 10, 15 or 30 μM ziritaxestat (MCE MedChemExprress) or sera from SLE patients at 1:2 ratio for indicated times. A summary of all inhibitors used in this paper and their on- and off- known targets is included as a Table 1.

**Table 1.**

| Family | Inhibitor | Target | Off-targets | Concentration used | pDC viability |
|---|---|---|---|---|---|
| JAK | AZD1480 | JAK2 | cell death > 1 μM | 1 μM | reduced (Figure S6B) |
| | baricitinib | JAK2/1 | NR | 25 nM-1 μM | reduced (Figure S6G) |
| | tofacitinib | pan JAK | NR | 200 ng/ml | reduced (not shown) |
| System LAA | BCH | SLC7A5 | SLC7A8 | 10 mM | NA |
| | JPH203 | SLC7A5 | NR | 5-10 μM | reduced at 10 μm (not shown) |
| System $x_c^-$ | erastin | SLC7A11 | VDACs | 5-10 μM | not affected (Figure S6B) |
| | sulfasalazine | SLC7A11 | NFκB | 100-200 μM | not affected (Figure S6B) |
| mTORC | rapamycin | mTORC1 | mTORC2 > 20 nM | 20 nM | not affected (not shown) |
| | torin 1 | mTORC1/2 | NR | 250 nM | reduced (not shown) |
| Glycolysis | heptelidic acid | GAPDH | NR | 10 μM | not affected (not shown) |
| OXPHOS | oligomycin | ATP synthase | NR | 1 μM | not affected (not shown) |

List of inhibitors used in the paper indicating inhibitor targets and off-targets, concentration used in this study and their effects on cell viability. NR stands for none reported, NA stands for not applicable.

## Flow cytometry

The following fluorochrome-conjugated monoclonal antibodies were used for staining cell surface markers: IL-3Rα (CD123, Miltenyi Biotec, clone AC145), HLA-DR (BD Bioscience, clone G46-6), CD303 (BDCA2, BioLegend, clone 201A), CD116 (BD Bioscience, clone hGMCSFR-M1), CD4 (BioLegend, clone A161A1). Whole PBMC-staining was performed in 0.5% BSA in PBS for 30 min at 4°C, dead cells were excluded with the LIVE/DEAD Fixable Near-IR Dead Cell Stain Kit (Invitrogen). Isolated pDC staining was performed in 0.5% BSA in PBS for 10 min at RT, dead cells were excluded with the LIVE/DEAD Fixable Near-IR or Aqua Dead Cell Stain Kits (Invitrogen). Unspecific binding was blocked with FcR blocking reagent (Miltenyi Biotec). The following fluorochrome-conjugated Abs were used for intracellular staining: IFN-α (Miltenyi Biotec, LT27:295), TNF (BioLegend, clone Mab11), pS6 (S235/236; CST, clone D57.2.2e), pSTAT5 (Y694; CST, clone C71E5). After surface staining, cells were fixed using Fixation/Permeabilization Kit (BD Bioscience) for 20 min at 4°C, and then additionally permeabilized in Perm/Wash solution for 30 min at 4°C, after which cells were incubated with antibodies against intracellular proteins, at previously determined antibody dilutions, for 30 min at RT.

De novo protein synthesis was measured using Click-iT Plus OPP Alexa Fluor 647 Protein Synthesis Assay Kit (Invitrogen) on pDCs stained with LIVE/DEAD Fixable Aqua Dead Cell Stain Kit (Invitrogen). Cycloheximide (Sigma) at 100 μg/ml was used as a positive control for protein synthesis inhibition.

Kynurenine uptake was performed using pDCs stained with antibody against IL-3Rα (Miltenyi Biotec) and LIVE/DEAD Fixable Near-IR Dead Cell Stain Kit (Invitrogen), as described previously (Sinclair et al., 2018). Briefly, stained cells were incubated in HBSS (GIBCO) with 200 μM kynurenine (Sigma) for 4 min at 37°C. Cells were then fixed and additional intracellular staining was performed as described above. Where indicated, at the time of kynurenine uptake, cells were treated with 10 mM BCH (Tocris). The 405 nm laser and 450/50 BP filter were used for kynurenine fluorescence detection.

Detection of intracellular mRNAs was performed using PrimeFlow RNA Assays according to manufacturer's protocol (Thermo scientific). Briefly, isolated pDCs were stained using LIVE/DEAD Fixable Aqua Dead Cell Stain Kit (Invitrogen) and fixed with fixation buffer I. Where indicated, cells were intracellularly stained with IFN-α and/or TNF in perm/wash buffer at previously determined concentrations. Then cells were fixed with fixation buffer II. Next, target-specific probes (*IFNA2* (type 6, 10), *TNF* (type 1), *SLC7A5* (type 6), *SLC3A2* (type 4), *SLC7A11* (type 1), *ENPP2* (type 4), *MYO1E* (type 6), *CCL3* (type 1), *CCL17* (type 6), *CXCL8* (type 1), *CXCL9* (type 1), *CXCL10* (type 1)) were hybridized to the target RNA transcript and signal was amplified. All buffers and times of incubation were provided by the manufacturer.

In all cases, cells were analyzed using LSR Fortessa flow cytometers (BD Biosciences) and data were processed using FlowJo software v.9.9.6 (Tristar).

## Cytokine and chemokine measurements

Isolated pDCs were plated at $1x10^6$/ml and incubated in RPMI (GIBCO) supplemented with 10% FBS (HyClone), 2 mM L-glutamine (GIBCO), 10,000 U/ml Penicillin/Streptomycin (GIBCO), 55 μM β-Mercaptoethanol (Sigma) containing 50 ng/ml recombinant human IL-3 (Perprotech) and 5 μM CpG-A (InvivoGen) for 24 hours. Where indicated cells were treated with either AZD or BAR (both at 1 μM, Selleckchem). Type I IFN (IFN-α, IFN-β, IFN-λ), TNF, CXCL8 and CXCL10 secretion was measured from supernatants using the LEGENDplex human Anti-Virus responses panel (Biolegend, #7410390) according to the manufacturer protocol.

## Metabolic assays

Extracellular acidification rate (ECAR) and oxygen consumption rate (OCR) were measured using mitochondrial stress test in a 96 well Extracellular Flux Analyzer (Seahorse Bioscience). Cells were plated at $0.15x10^6$ per well (coated with poly-D-lysine) and preincubated at 37°C for a minimum of 45 min in the absence of $CO_2$ in un-buffered RPMI (GIBCO) with 25 mM glucose (Sigma), 1 mM

pyruvate (Invitrogen) and 2 mM L-glutamine (GIBCO). Medium was supplemented with 10% FBS (HyClone) and 50 ng/ml recombinant human IL-3. (Peprotech). OCR and ECAR were measured under basal conditions following the addition of CpG-A. Results were collected with Wave software version 2.4 (Agilent). In Figure 2B, ECAR was measured in real time first in the absence of glucose and then following the addition of 10 mM glucose (Sigma). In this case data is presented as baseline-corrected.

Glucose and lactate were measured in cell culture supernatants using the Cedex Bio Analyzer (Roche) and data presented as mmol/L.

### Stable-isotope tracing

Sample preparation and metabolite extraction: 10 mM uniformly-labeled $^{13}$C-glucose (Sigma) was used to label isolated pDCs maintained in RPMI (GIBCO) supplemented with 10% FBS (HyClone), 2 mM L-glutamine (GIBCO), 10,000 U/ml Penicillin/Streptomycin (GIBCO), 55 μM β-Mercaptoethanol (Sigma) and 50 ng/ml recombinant human IL-3 (Peprotech) for 3 h. For metabolite analysis, 0.6x10$^6$ pDCs were washed in ice-cold PBS (GIBCO) and metabolites were extracted using 30 μL extraction buffer (50:30:20, methanol:acetonitrile:water, Sigma) cooled on dry ice for 30 min beforehand. Samples were centrifuged at 2000 g for 3 min to remove protein debris and supernatants were stored at −80°C until acquisition.

Metabolite measurement by LC-MS: LC-MS was carried out using an Agilent 1290 Infinity II UHPLC in-line with a Bruker Impact II QTOF operating in negative ion mode. Scan range was from 30 to 1050 Da. Mass calibration was performed at the beginning of each run. LC separation was on a Phenomenex Luna propylamine column (50 × 2 mm, 3 um particles) using a solvent gradient of 100% buffer B (5mM ammonium carbonate in 90% acetonitrile) to 90% buffer A (10 mM NH4 in water). Flow rate was from 1000 to 750 μl/min. The Autosampler temperature was 5°C and injection volume was 2 μl. Metabolites were quantified using AssayR (Wills et al., 2017), and identified by matching accurate mass and retention time to standards.

### scRNA-seq

Single cell RNA sequencing was performed using a 10X Genomics Chromium Controller. Single cells were processed with GemCode Single Cell Platform using GemCode Gel Beads, Chip and Library Kits (v2) following the manufacturer's protocol. An estimated 1400 cells were sequenced (~700 from each condition), with a mean of 64338 reads per cell and a mean of 2200 genes detected per cell. Libraries were sequenced on HiSeq 3000 (Illumina). Samples were demultiplexed and aligned using Cell Ranger 2.2 (10X Genomics) to genome build GRCh38 to obtain a raw read count matrix of barcodes corresponding to cells and features corresponding to detected genes. Raw read count matrices from single cell RNA sequencing data from lupus nephritis patients were retrieved from ImmPort:: SDY997 where the ethical approval, sample acquisition and preparation, as well as library processing is described in detail (Arazi et al., 2019).

Read count matrices were processed, analyzed and visualized in R using Seurat v. 3 (Stuart et al., 2019) and Uniform Manifold Approximation and Projection (UMAP) (McInnes et al., 2018) as a dimensionality reduction approach. Differentially expressed genes, with greater than a 1.2 fold change and an adjusted p value of less than 0.05, were obtained and compared across clusters using the UpSet methodology (Conway et al., 2017).

### Data and software availability

Single cell RNA sequencing data can be accessed at GEO: GSE157305.

### ChIP sequencing analysis

STAT5 binding sites were identified by retrieving raw sequencing data from Gene Expression Omnibus (GEO: GSE43119), which was produced from human T cells (Schmidl et al., 2014). The analysis performed was limited specifically to conventional T cells (samples SRR639410 and SRR639408). Retrieved data were processed using the default settings of the snakePipe methodology developed by the Bioinformatics core at the Max-Planck-Institute for Immunobiology and Epigenetics (Bhardwaj et al., 2019) which is described in https://snakepipes.readthedocs.io/en/latest/index.html. Samples were mapped to GRCh38 and binding sites were identified using MACS2 (Zhang et al., 2008) with the input control used as background.

### Tissue Immunostaining

Immunostaining for SLC7A11 and IL3-Rα (CD123) was performed on paraffin sections (6 mm). First, they were deparaffinized by xylol and ethanol incubations and washed in Tris-buffered saline (TBS). Heat-induced epitope retrieval was performed using Tris-EDTA buffer (10 mM Tris, 1 mM EDTA, pH 9) for 20 min in a heated (95°C) water bath. Samples underwent incubation with primary antibodies against SLC7A11 (Abcam, ab37185), and IL-3Rα (Novocastra/Leica, clone BR4MS, name NCL-L-CD123) diluted in TBS, 1% normal goat serum and 0.01% Tween in a humid chamber o/n at 4°C. For the immunofluorescence, Alexa Fluor 488 conjugated secondary antibodies were used. Cell nuclei were counterstained with DAPI. Immunohistochemistry was performed in an automated system (Leica BOND-MA, Leica Microsystem, Wetzlar, Germany). Images were captured using a BIOREVO BZ-9000 fluorescence microscope and associated software (Keyence, Neu-Isenburg, Germany).

### CRISPR-Cas9 mediated gene deletion:

RNP complexes were prepared by annealing (5 min, 98°C) equimolar amounts of crRNA and tracrRNA (180 pmol each per donor, IDT), followed by incubation with 60 pmol Alt-R S.p. Cas9 Nuclease V3 (IDT). Two separate crRNAs per target were used and mixed.

RNPs were delivered into purified human pDCs by electroporation in P4 Primary Cell buffer (Lonza) in the presence of 2 μM enhancer (IDT) using the CM-137 program (4D-Nucleofector, Lonza). Cells were allowed to recover for 1 h in recovery medium (Lonza) and rested in RPMI (GIBCO) supplemented with 10% FBS (HyClone), 2 mM L-glutamine (GIBCO), 10,000 U/ml Penicillin/Streptomycin (GIBCO), 55 μM β-Mercaptoethanol (Sigma) and 50 ng/ml recombinant human IL-3 (Peprotech) for 72 h prior to stimulation with CpG-A. The following guides were used: Hs.Cas9.SLC7A11.1.AA, Hs.Cas9.SLC7A11.1.AE, Hs.Cas9.SLC7A5.1.AA, Hs.Cas9.SLC7A5.1.AC, Hs.Cas9.SLC3A2.1.AB, Hs.Cas9.SLC3A2.1.AE, Hs.Cas9.GCGAGGTATTCGCTCCGCG (non-targeting control).

## QUANTIFICATION AND STATISTICAL ANALYSIS

With the exception of scRNA-Seq, statistical analysis was performed using Prism 7 software (GraphPad) and results are represented as mean ± SD or geometric SD (indicated in legends). Comparisons for two groups were calculated using unpaired two-tailed Student's t tests (Figures 1A, 1J, 2D, and 2E; Figures S1D, S1G, S1H, S2B, and S3D). Comparisons of more than two groups were calculated using one-way paired (Figures 1B, 1E–1I, 1K, 1L, 2A, 2F–2I, 3A, 3F, 3G, 5K, 5L, 6A (TNF), 6D, 6F, 6G, and 6J; Figures S1B, S1E, S1F, S2D, S3G, S3H, S3J, S3L, S5Q, S6C, S6E) or nonmatched (Figures 3B, 3D, 3E, 3I, 4A–4E, 4H, 5H, and 6A (IFN-α); Figures S3I, S3K, S4D, S4E, S4G, S4I, S5P S6A, S6B, and S6D) ANOVA with Tukeys multiple comparison tests or two-way paired (Figures 5M, 6E, 6H, and 6I; Figures S3F, S4B, and S4C) or nonmatched ANOVA (Figures 1D, 3C, 3H, 4F, 4G, 4I, 4J, 5J, 6C, 6K, and 6L; Figure S3E) with Tukeys multiple comparison tests. Designation of p values were as follows: * ≤ 0.05; ** ≤ 0.01; *** ≤ 0.001; **** ≤ 0.00001, ns - not significant.